What a Little Branching Can Do – Dissociative Photoionization of Two Butanol Isomers

Krisztián G. Torma,[a] Krisztina Voronova,[b] Amelia W. Ray,[a] Andras Bodi,[c] Bálint Sztáray,[a,*]

[a]*Department of Chemistry, University of the Pacific, Stockton, CA 95211, USA*

[b]*Department of Chemistry, University of Nevada, Reno, Reno, NV 89557, USA*

[c]*Laboratory for Synchrotron Radiation and Femtochemistry, Paul Scherrer Institute, CH-5232 Villigen PSI, Switzerland*

Abstract

The fragmentation processes of two internal energy-selected $C_4H_{10}O^+$ isomers, 1-butanol and isobutanol cations, were investigated by imaging photoelectron photoion coincidence (iPEPICO) spectroscopy. The first dissociation channel leads to the formation of $C_4H_8^+$ ions (*m/z* 56) by water loss in both isomers. Using statistical energy distribution and rate models including the isomerization of the parent ion, the 0 K appearance energies (E_0) were determined to be 10.347 ± 0.015 eV and 10.57 ± 0.05 eV for 1-butanol and isobutanol, respectively. The second dissociation channel, the formation of $CH_3OH_2^+$, quickly overtakes the water-loss channel in isobutanol with an E_0 of 10.61 ± 0.02 eV. It appears only as a minor channel in 1-butanol with an E_0 of 10.74 ± 0.09 eV. The methanol-loss channel, forming propylene ion, opens up at E_0 = 10.94 ± 0.04 eV and 10.72 ± 0.02 eV in 1-butanol and isobutanol, respectively. The next two fragmentation pathways correspond to complementary pair formation of $C_3H_7^{(+/o)}$ and $CH_2OH^{(o/+)}$. The former is assigned as the isopropyl (ion) in both butanol isomers. The channel corresponds to simple bond cleavage in isobutanol with the E_0 differences corresponding to the ionization energy difference of the fragments at E_0 = 10.97 ± 0.05 eV ($C_3H_7^+$) and at E_0 = 11.11 ± 0.20 eV (CH_2OH^+). However, there is an internal hydrogen shift necessary in 1-butanol and, therefore, the complementary ions appear at the same E_0 = 11.10 ± 0.03 eV, which corresponds to a shared rate limiting transition state. The sequential dissociation product from *m/z* 56, $C_3H_5^+$, appears above 11.6 eV as a minor channel in both isomers. Finally, we determined –279.10 ± 1.64 kJ mol^{-1} as the 298 K heat of formation of gaseous isobutanol.

[*]Author to whom correspondence should be addressed. Email: bsztaray@pacific.edu

Introduction

Butanols are derived from lignocellulosic materials and are among the most promising biofuel alternatives to ethanol. Although bioethanol is used as a fuel additive in numerous countries, butanols, and 1-butanol in particular, have several advantages: lower water uptake, higher energy density, better mixing with common fuels, and better compatibility with traditional engines.[1] With the exception of *tert*-butanol, all butanol isomers can be produced from renewable sources, making them ideal biofuels.[2]

The four butanol isomers have been the subject of experimental studies with a focus on their viability as a fuel. These include investigations of their chemistry at high temperature, relevant to combustion conditions, including species profile,[3-4] laminar flame speed,[5-6] and ignition delay times.[7-10] These studies were carried out in jet stirred reactors,[11-12] flames,[13-15] and pyrolysis.[3-4,16] Kinetic models have been proposed to explain the combustion chemistry of butanol isomers and to fit experimental data.[10-12,16-17] Although many of these species and elementary reactions involved have been fairly well characterized, thermochemical input parameters are one of the major source of uncertainty in combustion models.[18-20] Unfortunately, the gas phase heats of formation of the butanol isomers remain poorly known. For 1-butanol, NIST[21] reports an average value –277 ± 5 kJ mol^{-1} as the 298 K gas phase heat of formation. None of the included 13 measurements is more recent than 1975 and most of them were concerned with the liquid phase, converted to the gas phase using the heat of vaporization by Skinner and Snelson[22] and Wadsö.[23] The enthalpy of formation of gaseous 1-butanol was reported in various other thermochemical databases: –274.9 ± 0.4 kJ mol^{-1} by Pedley et al.;[24] –274.4 kJ mol^{-1} by Rosenstock et al.;[25] and most recently (in 2006) as –274.6 kJ mol^{-1} by Yaws.[26] However, none of these evaluations is based on new experimental data. Isobutanol has been less studied and the most recent 298 K gas phase heat of formation, –283.8 ± 0.9 kJ mol^{-1}, by Connett dates back to 1975.[27] This value was determined using the measured heat of formation of liquid isobutanol by Skinner and Nelson.[22] Rosenstock et al.[25] reported this value, and Pedley et al.[24] reported –283.8 ± 0.8 kJ mol^{-1}.

Photoelectron photoion coincidence (PEPICO) spectroscopy coupled with vacuum ultraviolet (VUV) synchrotron radiation enables the measurement of highly accurate thermochemical data of a wide variety of systems.[28-29] In a threshold PEPICO dissociative photoionization experiment, the threshold photoionization signal corresponding to a given photoion *m/z* is recorded. Then, fractional ion abundances are plotted as a function of the photon energy in the breakdown diagram, which is modeled with statistical energy distributions and unimolecular rates to extract thermochemical information, *i.e.,* fragment ion appearance energies. Our motivation is to revisit the dissociative photoionization of 1-butanol and isobutanol to quantitatively understand the ionic dissociation processes.

The dissociation mechanism of the butanol isomer cations and the possible fragment ions have been discussed in the literature at length.[30-33] McAdoo and Hudson[30] studied the water-loss channel from the 1-butanol cation and the deuterated analogs using photoionization mass spectrometry. Deuterium-labeled 1-butanol led to the loss of both HDO and D_2O in varying amounts, depending on the original deuterium position. When hydrogens of only one carbon

atom were replaced with deuterium, the observed amount of HDO loss was similar for all 4 carbon, slightly lower than the statistical predictions, roughly in line with the expected isotope effect. These results led McAdoo and Hundson[30] hypothesize that 1-butanol isomerizes by extensize hydrogen transfers within the ion–neutral complex $^{+}CH_2CH_2CH_2CH_2\ldots OH_2$. They also proposed that $CH_2CH_2CH_2CH_2OH_2^+$ may isomerize reversibly into a cyclobutane ion–water complex, essentially rendering all hydrogen atoms equivalent. According to them, this would also explain the experimentally observed hydrogen exchanges.

Shao et al.[31] studied the H_2O-loss channel using photoelectron photoion coincidence spectroscopy (PEPICO). In the 9.8–10.2 eV photon energy range, only the water-loss fragment ion, $C_4H_8^+$ (*m/z* 56) was detected. They theorized that a complex reaction mechanism must be involved yielding the *trans*-2-butene ion, the most stable $C_4H_8^+$ isomer, as well as the methylcyclopropane ion. The formation of both products involves a rearrangement of the 1-butanol molecular ion to an ion–neutral complex of the 2-butene ion and water or the methylcyclopropane ion and water. They could not determine the energy of these ion–neutral complexes, but suggested that the formation of the methylcyclopropane ion is a slow process, and the formation of the *trans*-2-butene ion is a fast process. The appearance energy (E_0) of $C_4H_8^+$ was determined to be 10.18 ± 0.05 eV, in agreement with the electron impact value of 10.20 ± 0.05 eV by Bowen and Maccoll,[34] and with the E_0 of 10.19 ± 0.05 eV, determined by Xie et al.[32] using photoionization mass spectrometry. Two minor fragment ions were also observed by Xie et al.,[32] but with only a small contribution to the total photoionization cross-section of 1-butanol. The E_0 of *m/z* 42 ion, $C_2H_2O^+$, was determined to be 11.10 ± 0.05 eV, and the E_0 of *m/z* 31, CH_3O^+, was determined as 11.30 ± 0.05 eV, in agreement with the values of 11.23 ± 0.1 eV by Lambdin et al.[35] and 11.40 ± 0.06 eV by Selim and Helal,[36] respectively.

Shao et al.[31] reported the dissociative photoionization mechanism of isobutanol to be even more complex than that of 1-butanol. Four major fragments were detected in the photon energy range of 9.6–12.4 eV, in agreement with the findings of Xie et al.,[32] out of which the first two, *m/z* 56 and *m/z* 33, were found to be slow dissociation processes. The water loss channel yielding *m/z* 56, $C_4H_8^+$, is weak and quickly overtaken by the other slow channel, the formation of $CH_3OH_2^+$ (*m/z* 33). Shao et al.[31] suggested that the water loss channel proceeds solely via the formation of a methylcyclopropane–water complex. The appearance energy of the *m/z* 56 ion was given as 10.33 ± 0.03 eV. Xie et al.[32] determined an E_0 of 10.32 ± 0.05 eV for this channel. The *m/z* 33 channel, $CH_3OH_2^+$, is a major fragment with reported appearance energies of 10.43 ± 0.03 eV[31] and 10.36 ± 0.05 eV.[32] The other two fragment ions reported, $C_3H_6^+$ (*m/z* 42) and $C_3H_7^+$ (*m/z* 43), are consistent with the loss of methanol and the loss of CH_2OH, respectively. The *m/z* 42 channel is the lower energy path, but it includes an isomerization step, and is overtaken by the $C_3H_7^+$ channel at higher energies, which only requires direct C–C bond cleavage. Appearance energies of $C_3H_6^+$ were determined to be 11.00 ± 0.03 eV and 10.81 ± 0.05 eV, and of $C_3H_7^+$ was found to be 11.28 ± 0.05 eV and 11.00 ± 0.05 eV, by Shao et al.[31] and Xie et al.,[32] respectively. Although Xie et al.[32] noted that their values are consistently lower than that of Shao et al.'s,[31] they gave no explanation on what may cause the discrepancy.

We have investigated the dissociative photoionization of two internal energy selected butanol isomer cations using imaging photoelectron photoion coincidence (iPEPICO) spectroscopy at the Swiss Light Source (SLS). The two parent ion isomers, 1-butanol and isobutanol cations, dissociate into fragment ions with the same set of masses but the relative abundance of these fragments differs widely between the two very similar species. In contrast, in, *e.g.,* dichloroethylene isomers, the dissociative photoionization sets in at energies at which the isomer parent ions readily interconvert, *i.e.,* lose their isomeric identity.[37] Maybe there is such a threshold in the butanol isomers as well, although probably not below the dissociative photoionization onset. Hence, in addition to generating new experimental thermochemical data or confirming existing thermochemistry, our analysis shall offer insights into the dissociation mechanisms that may be qualitatively different between the two systems.

Experimental and Theoretical Approach

Experimental

1-Butanol (99.7%) and 2-methyl-1-propanol (isobutanol, 99.5%) were purchased from Sigma–Aldrich and used without further purification. Both room temperature samples were introduced through an effusive inlet into the ionization chamber of the iPEPICO endstation[38] at the VUV beamline[39] of the Swiss Light Source. The pressure of the experimental chamber was set to 1–3 × 10^{-6} mbar. VUV synchrotron radiation was used to ionize the samples in a 2 × 2 mm^2 interaction region with a photon energy resolution of 3–5 meV. Photoions and photoelectrons were extracted in opposite directions from the ionization region using a constant 120 V cm^{-1} electric field. Photoelectrons were velocity-map-imaged onto a Roentdek DLD40 position-sensitive delay-line detector from which two regions were utilized. First, threshold electrons were focused to the center of the detector, together with kinetic energy ("hot") electrons with no off-axis momentum. Second, hot electrons with an off-axis momentum were accounted for based on the signal in a ring around the center spot. Hot electron contribution to the threshold photoelectron signal was removed by subtracting the average signal counts in the ring region from that of the center signal using an appropriate scaling factor to account for area and collection efficiency differences.[40] Photoions were mass analyzed by a two-stage Wiley–McLaren[41] time-of-flight (TOF) mass spectrometer and were spaced-focused onto a Jordan TOF C-726 microchannel plate detector. The start signal for the TOF analysis of the photoions is provided by photoelectron detection events in a multiple-start/multiple-stop coincidence data acquisition scheme.[42] Ion residence times in the first acceleration region are on the order of microseconds due to its length and the low extraction field. If an ion dissociates in this region, the time of flight of the resulting fragment ion will be somewhere between the nominal TOF of the parent and the fragment ions. The fragment ion peak due to a slow dissociation will exhibit a broad, quasi-exponential shape toward higher *m/z* ratios, indicative of the unimolecular rate constant of dissociation.[43-44] Dissociation rates of 10^3 – 10^7 s^{-1} can be measured and fitted to the modeled rates, quantifying the kinetic shift[45] and providing a reliable extrapolation to the dissociation threshold.

Statistical Modeling

The experimental breakdown diagram and the threshold ionization TOF mass spectra with asymmetric peak shapes were modeled using rigid activated complex Rice–Ramsperger–Kassel–Marcus (RAC-RRKM) theory.[43,46] These calculations were used to extract the experimental rate constants from the experimental time-of-flight data by fitting the calculated peak shapes to the quasi-exponential asymmetric fragment ion peaks. We calculated the molecular ion's internal energy distribution and the dissociation rate constants, based on which ion branching ratios (breakdown diagram) and TOF spectra were calculated and compared to the experimental data. The RAC-RRKM unimolecular rate constants for each dissociation pathway, $k(E)$, were calculated by the following formula

$$k(E) = \frac{\sigma N^{\ddagger}(E - E_0)}{h\rho(E)} \quad (1)$$

where σ represents the symmetry number of the fragmentation channel, h is Planck's constant, $N^{\ddagger}(E - E_0)$ is the number of states function for the transition state at internal energy $E - E_0$, and $\rho(E)$ is the density of states for the dissociating ion at internal energy E. The sums and densities of states were calculated using harmonic vibrational frequencies by the Beyer–Swinehart direct count algorithm.[47]

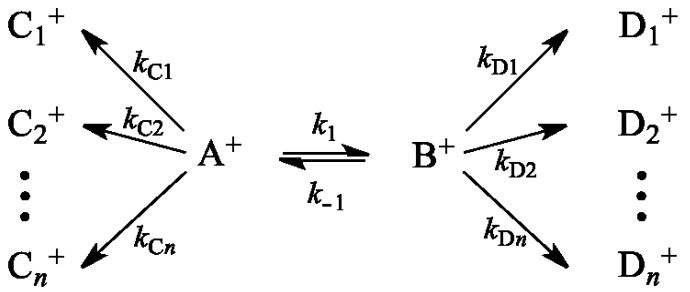

Figure 1. Isomerization of A^+ molecular ion to B^+ and their fragmentation to $C_1^+ \ldots C_n^+$ and $D_1^+ \ldots D_n^+$ ions, respectively.

The molecular ion may undergo reversible isomerization prior to dissociation.[48-55] Product ions can be formed from either the parent ion or from its isomer. Let us consider a hypothetical system, shown in Figure 1, where A^+ molecular ion reversibly isomerizes to B^+, and A^+ dissociates to ($C_1^+ \ldots C_n^+$) and B^+ to ($D_1^+ \ldots D_n^+$) fragment ions, respectively. Solutions of the rate equations are discussed in details elsewhere.[43] In short, in the case of two molecular ion isomer structures, each fragment ion is formed with two apparent rate constants, k_{fast} and k_{slow}, which can manifest themselves in the TOF spectra as double-exponential asymmetric fragment ion peaks. Therefore, such features in the experimental TOF spectra indicate that isomerization is at play.

Quantum Chemistry

The analysis of the experimental data and the statistical modeling was aided by *ab initio* calculations, using the Gaussian 09 suite of programs.[56] Rotational constants and harmonic

vibrational frequencies at the B3LYP/6-311++G(d,p) level of theory were used to calculate the thermal energy distribution of the neutral, numbers and densities of states for the rate equation (1), and stationary point energies for examining the possible isomerization and dissociation pathways.[43] Stationary points for the most likely dissociative photoionization pathways and ion rearrangements were refined using the G4 composite method.[57] Transition state (TS) structures were located using constrained optimizations and synchronous transit-guided quasi-Newton calculations[58-59] and verified using intrinsic reaction coordinate (IRC) calculations. The ionization energy of 1-butanol and isobutanol have been calculated using further composite methods, namely CBS-QB3,[60-61] CBS-APNO,[62] and W1U[63].

Results and Discussion

Statistical Modeling of the Dissociative Photoionization Processes

Threshold photoionization time-of-flight mass spectra of internal energy selected 1-butanol and isobutanol ions were collected in the 10.0–13.2 eV photon energy range. We found that the dissociative photoionization of both 1-butanol and isobutanol generate fragment ions with *m/z* 31, 33, 41, 42, 43, and 56. The most likely fragmentation processes leading to these ions are shown in Scheme 1.

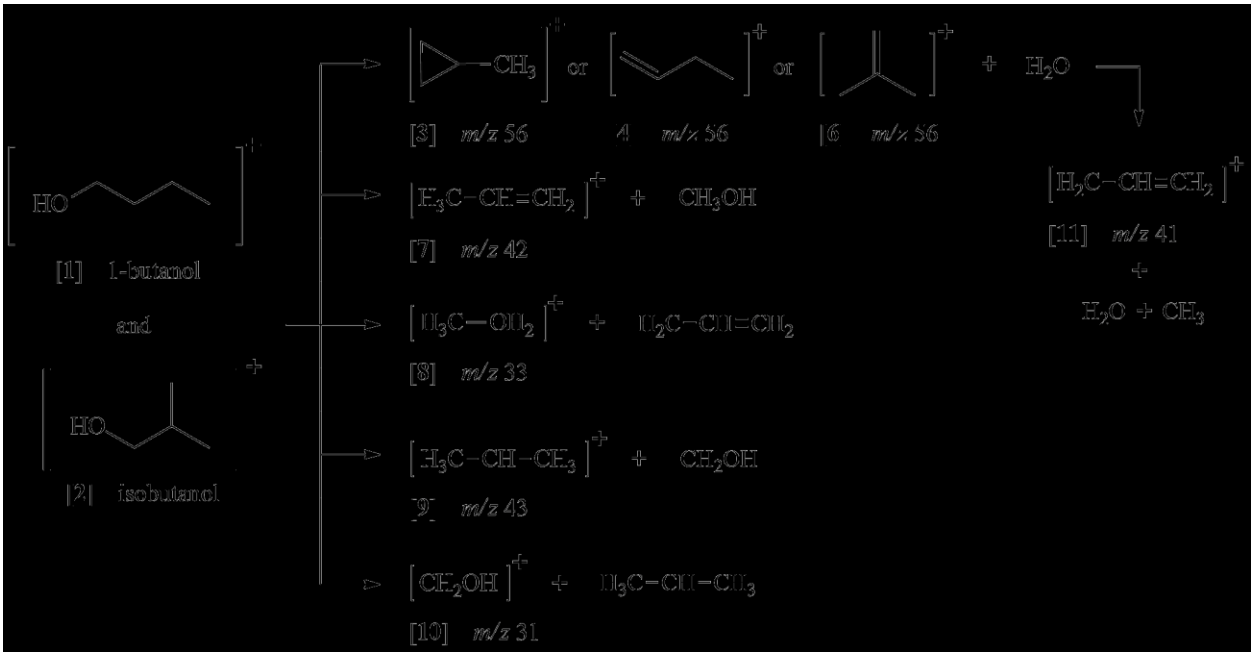

Scheme 1. General dissociation pathways of 1-butanol and isobutanol in the 10.0–13.2 eV photon energy range.

1-Butanol.

Reported adiabatic ionization energies (AIE) of 1-butanol vary between 9.95 and 10.10 eV, as listed in Table 1.[31-32,64] Our PEPICO measurement, however, shows significant

dissociation already at 10.0 eV, which implies that these literature values are too high. Determining the precise location of the onset of a photoionization mass spectrum (PIMS) involves extrapolation to the baseline with a straight line. The extrapolated energy depends on which region of the spectrum is fitted. Photoelectron spectroscopy is a more suited technique to determine the ionization energy than PIMS but low Franck–Condon factors for the origin transition can blue shift the ionization onset significantly. This has been shown for ethanol where the reported AIE values were found to be significantly higher than the true value.[65] A similarly large discrepancy but with an opposite sign has been observed between the previously published and the true AIE of diethyl ether.[66] Hence, we calculated the 1-butanol AIE at the G4,[57] CBS-QB3,[60-61] CBS-APNO,[62] and W1U[63] composite levels of theory (9.86_1, 9.86_3, 9.83_1, and 9.88_7 eV, respectively). All these values are in remarkably good agreement with each other but are lower than the literature values. Therefore, their average of 9.86 eV most likely represents a reliable theoretical estimate for the 1-butanol AIE and we used this value to calculate the internal energy distribution of the 1-butanol molecular ion in the statistical model. It is important to note that we measure the appearance energy of a fragment ion directly in PEPICO spectroscopy, variations in the AIE only affect the results indirectly by the way of the rate curve extrapolation in the statistical model.

Table 1. Summary of adiabatic ionization energies (AIE) and 0 K appearance energies (E_0) for the two butanol isomer cations and their fragment ions.

Species	E_0 (eV) Experimental[a]	AIE or E_0 (eV) Computed (G4)[a]	AIE or E_0 (eV) Literature
1–C_4H_9OH [1]		9.86 ± 0.05[b]	9.99 ± 0.05[c]
m/z 74			10.09 ± 0.02[d]
			9.95 ± 0.05[e]
CH_3–c–$C_3H_5^+$ [3]	10.347 ± 0.015	10.42	10.18 ± 0.05[c]
CH_2=CH–$C_2H_5^+$ [4]	10.95 ± 0.15		10.20 ± 0.05[f]
m/z 56			10.19 ± 0.05[e]
CH_3–CH=CH_2^+ [7]	10.94 ± 0.04	10.87	11.10 ± 0.05[e]
m/z 42			11.23 ± 0.1[g]
CH_3–OH_2^+ [8]	10.74 ± 0.09	10.51[i]	
m/z 33			
CH_3–CH–CH_3^+ [9]	11.10 ± 0.03	11.00	
m/z 43		10.99[i]	
CH_2OH^+ [10]	11.10 ± 0.03	11.05[i]	11.30 ± 0.05[e]
m/z 31			11.40 ± 0.06[h]
CH_2=CH–CH_2^+ [11]	11.6 – 11.7	11.63	
m/z 41			
i–C_4H_9OH [2]		9.66 ± 0.05[b]	10.02 ± 0.05[c]
m/z 74			10.09 ± 0.02[d]
			9.95 ± 0.05[e]
$CH_3C(=CH_2)CH_3^+$ [6]	10.57 ± 0.05	10.50	10.33 ± 0.03[c]
m/z 56			10.32 ± 0.05[e]
CH_3–CH=CH_2^+ [7]	10.72 ± 0.02	10.77[i]	11.00 ± 0.03[c]
m/z 42			10.81 ± 0.05[e]
CH_3–OH_2^+ [8]	10.61 ± 0.02	10.62[i]	10.43 ± 0.03[c]
m/z 33			10.36 ± 0.05[e]
CH_3–CH–CH_3^+ [9]	10.97 ± 0.05	11.09	11.28 ± 0.05[c]
m/z 43			11.00 ± 0.05[e]
CH_2OH^+ [10]	11.11 ± 0.20	11.15	
m/z 31			
CH_2=CH–CH_2^+ [11]	11.6 – 11.9	11.73	
m/z 41			

[a] This work. [b] Average computed AIE at the G4, CBS-QB3, CBS-APNO, and W1U levels. [c] Shao et al.[31] [d] Cocksey et al.[64] [e] Xie et al.[32] [f] Bowen and Maccoll.[34] [g] Lambdin et al.[35] [h] Selim and Helal.[36] [i] G4-calculated thermochemical limit.

The 1-butanol breakdown diagram is shown in Figure 2, along with selected TOF spectra in Figure 3. Below the photon energy of 10.8 eV, only the molecular ion, $CH_3CH_2CH_2CH_2OH^+$ (*m/z* 74) [1], and the first, water-loss fragment ion $C_4H_8^+$ (*m/z* 56) [3] were detected, in line with earlier photoionization studies. Based on the asymmetric fragment ion TOF peak shapes, shown in Figure 3, this dissociation pathway is "slow" near threshold; that is, the parent ion is metastable on the time scale of the experiment. The *m/z* 56 fragment ion can be formed via a hydrogen atom transfer to the OH group from one of the carbon atoms. In order to determine which hydrogen transfer pathway is responsible for this dissociation channel, extensive DFT geometry optimizations and G4 single-point energy calculations were carried out. These results are discussed in the Potential Energy Surface section (*vide infra*) and shown in Figure 4. In short, our calculations show that hydrogen transfer proceeds through transition states 0.14 to 1.42 eV above the molecular ion (10.00 to 11.28 eV relative to the neutral precursor), leading to lower energy isomeric structures that feature loosely attached ion···H_2O moieties, consistent with earlier literature findings.[30,33] The first step in the α-carbon hydrogen shift involves a transition state that is at 11.28 eV (*relative to the neutral precursor*), much too high to be relevant at threshold. H-atom transfer from the β-carbon features a similarly prohibitively high saddle point at 10.70 eV. However, for a γ-carbon H-atom shift, the CH_2OH moiety can first rotate closer to the γ-carbon and the hydrogen transfer happens through a transition state at already 10.42 eV. The subsequent loss of water produces the methylcyclopropane fragment ion with a calculated thermochemical limit of 9.87 eV. The δ-carbon hydrogen shift and subsequent water-loss follows the well-known McLafferty rearrangement mechanism[67] forming cyclobutane with an effective transition state 0.40 eV higher than the γ-carbon H-shift pathway.

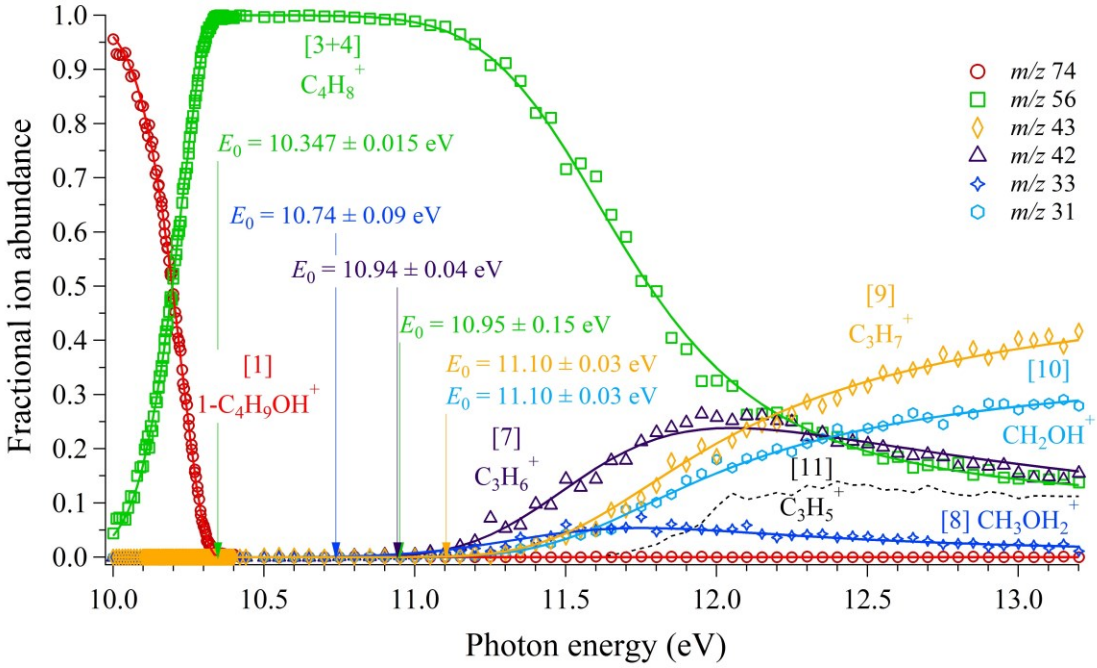

Figure 2. Breakdown diagram for 1-butanol in the 10.0–13.2 eV photon energy range. Polygons are experimentally measured ion abundances and the solid lines are the best-fit modeling of the data (*see text*).

The dashed line shows the fractional abundance of the *m/z* 41 ion, the consecutive dissociation of the *m/z* 56 ion which was not separated out in the statistical model and, therefore, the green polygons and line stand for the sum of the *m/z* 56 and 41 ions above 11.6 eV photon energy.

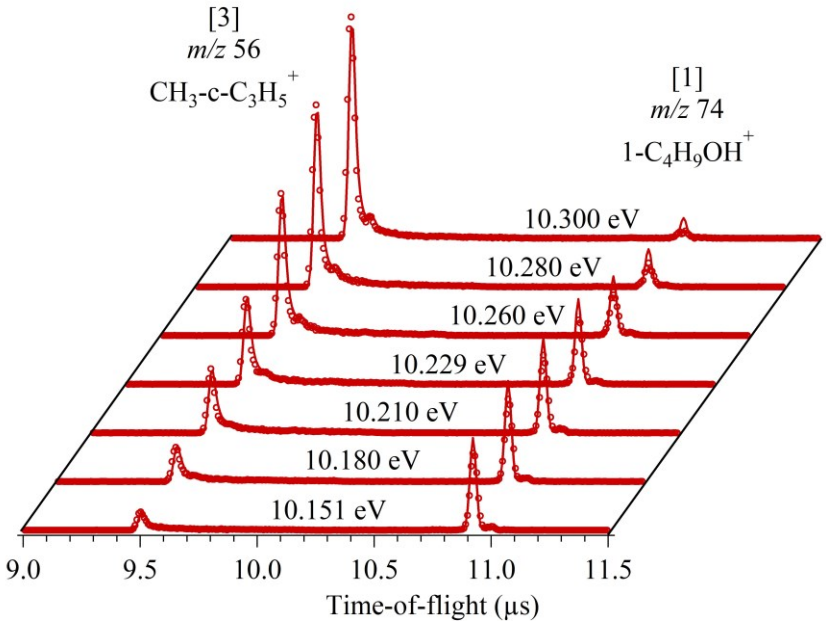

Figure 3. Selected threshold photoionization TOF distributions of 1-butanol. Open circles are the experimentally measured PEPICO TOF spectra and lines are the best fit modeling of the data. Note that the $[M+1]^+$ peak at 11.0 μs is the ^{13}C isotope contribution of 1-butanol.

As mentioned earlier, a double exponential fragment ion peak shape is a revealing sign that more than one isomeric structure plays an active role in the dissociation process.[43,54] Furthermore, the statistical modeling did not result in an acceptable fit to the experimental rate curve (manifested in the asymmetric TOF distribution data) when only using one parent ion structure. Therefore, the statistical model includes the molecular ion reversibly isomerizing into a methylcyclopropane···water ion-neutral complex isomeric structure. A tight transition state connects the 1-butanol molecular ion with the isomer structure reversibly and a loose TS serves as the exit channel. In fitting the model to the experimental TOF distributions and breakdown curves, we optimized the barrier height leading to dissociation and the lowest five frequencies of the corresponding loose TS structure, and the height of both the forward and reverse isomerization barriers. The isomerization transition state frequencies were calculated at the B3LYP level and were kept unchanged in the model. In the best fit of the data, the isomerization barrier height and the isomer stabilization energy (both relative to the molecular ion) were found to be 0.44 eV and –0.19 eV, respectively. The appearance energy of the water-loss *m/z* 56 (methylcyclopropane) fragment ion (E_0) was determined to be 10.347 ± 0.015 eV. This is in reasonable agreement with the G4 value of 10.42 eV and suggests that the lowest-energy water-loss channel of 1-butanol leads to the formation of methylcyclopropane ion. This is partially in line with the hypothesis of Shao et al.,[31] who assumed the formation of two $C_4H_8^+$ isomer cations:

trans-2-butene and methylcyclopropane. However, although *trans*-2-butene is the most stable $C_4H_8^+$ isomer, our quantum chemical calculations revealed no low-energy pathways to it and the most probable $C_4H_8^+$ structure is methylcyclopropane, not *trans*-2-butene (Figure 4).

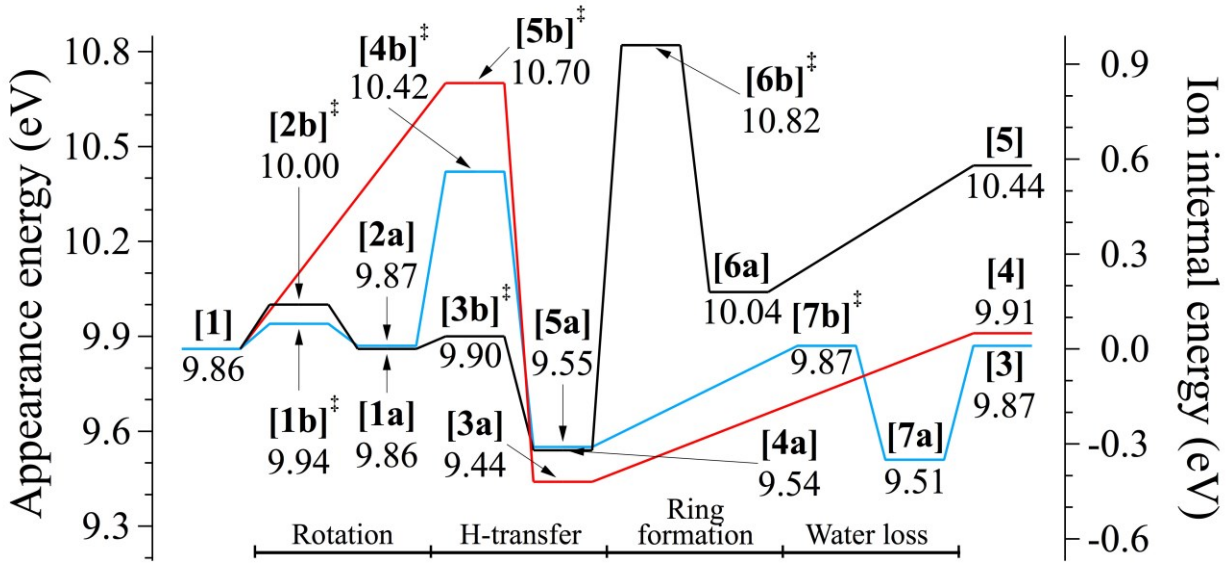

Figure 4. Potential energy surface for the internal hydrogen rearrangement and subsequent water loss from energy-selected 1-butanol ions. The pathways with beta, gamma, and delta-carbon hydrogen transfers are shown with red, blue, and black ink, respectively. Energies on the left axis are relative to the neutral precursor while energies on the right axis are relative to the molecular ion. All energies are at 0 K at the G4 level of theory. For structures, cf. Figure 10 and the schemes in the text.

Beyond 11 eV, four additional parallel dissociation channels open up at approximately the same photon energy: $C_3H_6^+$ (*m/z* 42, [7]) by methanol loss, $CH_3OH_2^+$ (*m/z* 33, [8]) by loss of C_3H_5, $C_3H_7^+$ (*m/z* 43, [9]) by loss of CH_2OH, and CH_2OH^+ (*m/z* 31, [10]) by C_3H_7 loss. Two of these dissociation channels, *m/z* 33 and 43, were not reported in earlier studies. These four channels were modeled in parallel with the *m/z* 56 channel, using calculated frequencies for the loose transition states as starting points and fitting both the transitional TS frequencies and the appearance energies to the experimental breakdown curves.

The formation of $C_3H_6^+$ (*m/z* 42, [7]) and $CH_3OH_2^+$ (*m/z* 33, [8]) fragment ions once again requires rearrangement of the 1-butanol cation prior to dissociation. Based on our quantum chemical calculations, the most likely structure of $C_3H_6^+$ is $CH_3CHCH_2^+$, formed by a γ-carbon hydrogen transfer to the α-carbon followed by the loss of a CH_3OH fragment. The calculated transition state for this pathway lies at 10.87 eV, in reasonable agreement with the experimentally derived appearance energy of 10.94 ± 0.04 eV. Xie et al.[32] reported a slightly higher value, 11.10 ± 0.05 eV, but, strangely, identified the *m/z* 42 ion as $C_2H_2O^+$. They provided no explanation, however, on the formation of this ion from 1-butanol molecular ion, which would require a C_2H_8 loss. According to our calculations, the formation of $CH_3OH_2^+$ proceeds

through a β-carbon hydrogen transfer to the OH group instead. Then, the water and the methyl group forms protonated methanol while CH_2CHCH_2 (allyl) neutral is lost. The experimentally derived E_0 is 10.74 ± 0.09 eV, which could not be corroborated with a G4 transition state energy as optimizations of this TS structure have not converged.

The next two fragmentation pathways correspond to a complementary pair: $C_3H_7^+$ (*m/z* 43, [9]) through the loss of CH_2OH, and CH_2OH^+ (*m/z* 31, [10]) through the loss of C_3H_7. If the appearance energies of these two channels correspond to their respective thermochemical limits, the difference in the E_0 values has to be equal to the ionization energy difference of the two neutral fragments, *i.e.,* C_3H_7 and CH_2OH, for which the ATcT[68] value is 0.110 ± 0.007 eV. However, the experimental 0 K appearance energies are equal within error bars at 11.10 ± 0.03 eV, suggesting that these reactions proceed through a common transition state, slightly above the thermochemical limits. This is not surprising since there is a necessary H-shift in order to form the most stable C_3H_7 isomer neutral or ion, CH_3CHCH_3. Calculated thermochemical limits of 10.99 and 11.05 eV for the formation of the $CH_3CHCH_3^+$ and CH_2OH^+ fragment ions, respectively, are indeed below the experimental onset. We identified their common transition state at 11.00 eV, which is only slightly higher than the thermochemical threshold of the isopropyl ion. Previously, Xie et al.[32] measured a somewhat higher value, 11.30 ± 0.05 eV for the appearance energy of the *m/z* 31 ion.

Finally, a sixth channel opens up around 11.7 eV, consistent with $C_3H_5^+$ formation (*m/z* 41, [11]). Since the formation of this ion requires an overall loss of CH_5O, it must be a product of sequential steps, *i.e.,* the methyl-loss product from the first, water-loss fragment ion, $C_4H_8^+$ (*m/z* 56). Our PEPICO modeling code is equipped to handle complex dissociation schemes with two isomer ions, several parallel dissociation channels and consecutive dissociations from one of those. However, according to theory, the situation is even more complicated here, due to the multiple possibilities on forming the *m/z* 56 fragment ion (*vide supra*).[43] Therefore, we were unable to determine a reliable experimental value for the appearance energy of the *m/z* 41 ion and, instead, its experimental ion abundances were summed into its parent ion and they were modeled together as one channel. Then, the high energy tail of this combined breakdown curve could not be reproduced with a single *m/z* 56 channel, which finding is in line with the quantum-chemical calculations but complicates the picture of how the *m/z* 41 fragment ion comes about. Therefore, a more complex model was built with two parallel $C_4H_8^+$ channels and this model provided an excellent fit to the combined *m/z* 56 and *m/z* 41 curve. According to the model, the contribution of the second H_2O-loss pathway never amounts to more than 15%. Therefore, it is not very sensitive to this second *m/z* 56 appearance energy, for which 10.95 ± 0.15 eV is our best estimate. This value is not far from the calculated transition state energy of 10.70 eV leading to the formation of the 1-butene fragment ion and while, from the experimental data alone, it is not possible to firmly address the energetics of this second *m/z* 56 channel, its existence is quite clear.

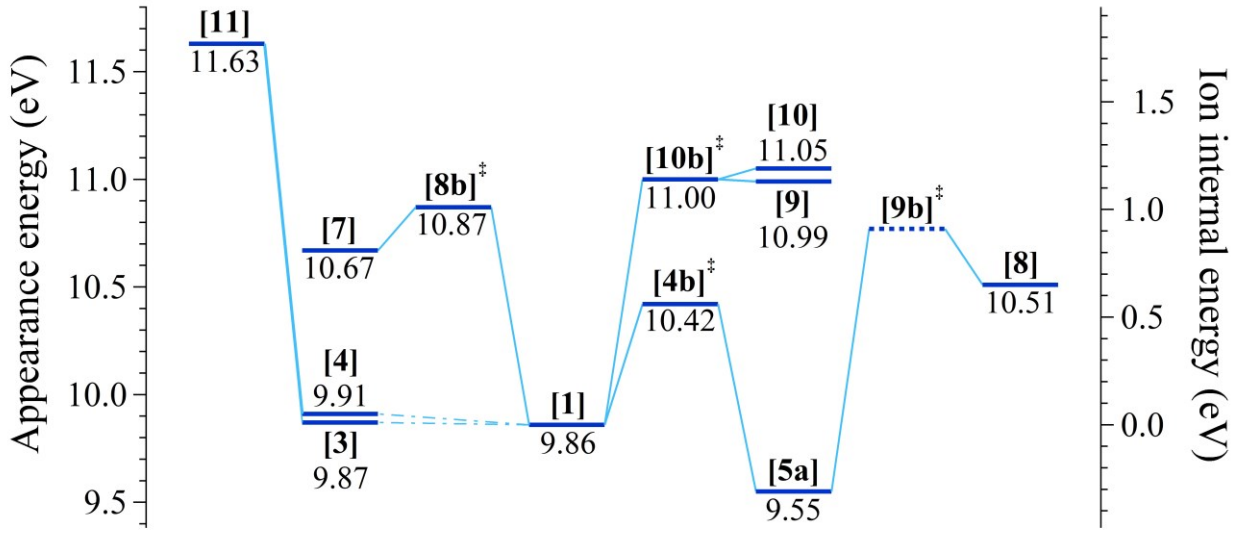

Figure 5. G4-calculated potential energy surface for the remaining dissociation pathways of energy-selected 1-butanol ions. Energies on the left axis are relative to the neutral precursor while energies on the right axis are relative to the molecular ion. For structures, see Figures 10, 11, and the schemes in the text.

Isobutanol

The AIE of isobutanol was reported to be between 9.95 and 10.12 eV with typical uncertainties of 0.05 eV.[31-32,64] Similarly to the case of 1-butanol (*vide supra*), we calculated the isobutanol AIE at the G4,[57] CBS-QB3,[60-61] CBS-APNO,[62] and W1U[63] composite levels of theory (9.65_6, 9.68_6, 9.63_3, and 9.68_7 eV, respectively). As the precision of our calculated values is impressive, and they are significantly lower than the experimental data found in the literature, it is possible that literature values do not correspond to the adiabatic value. Therefore, we used the 9.66 ± 0.05 eV in the statistical modeling of the isobutanol PEPICO data.

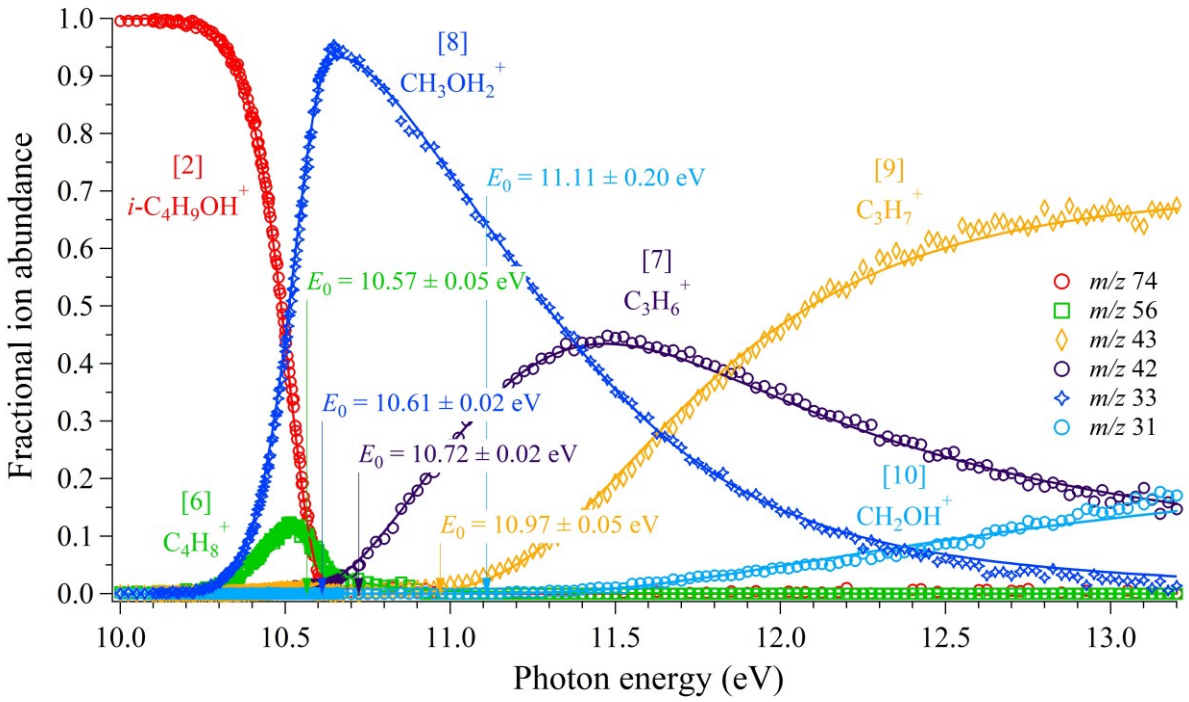

Figure 6. Breakdown curves for isobutanol in the 10.0–13.2 eV photon energy range. Solid polygons correspond to experimental data points, whereas continuous lines are modeling results. The *m/z* 41 channel is not included here because of its low abundance.

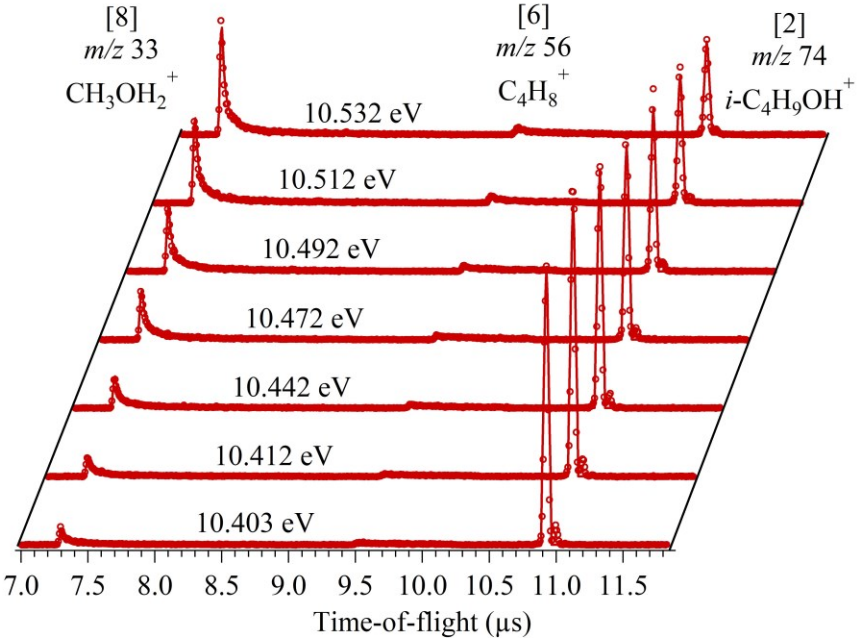

Figure 7. Representative threshold photoionization TOF mass spectra of isobutanol. Open circles are the experimentally measured data points, lines are the best fit modeling of the data. Note that the $[M+1]^+$ peak at 11.0 μs is the ^{13}C isotope contribution of isobutanol.

The breakdown diagram of isobutanol is shown in Figure 6 and selected PEPICO time-of-flight spectra are shown in Figure 7. Compared to 1-butanol, the breakdown diagram for isobutanol consists of the same six fragment ions, but with the notable difference that the lowest energy H_2O-loss channel is no longer the only low-energy channel. Similarly to 1-butanol, two dissociation channels, the formation of *m/z* 31 and 41 are first reported here.

The first channel involves a loss of water to produce $C_4H_8^+$ (*m/z* 56, [3,4,6]). In contrast to 1-butanol, the water-loss channel is much less abundant and is quickly overtaken by the loss of C_3H_5 to produce $CH_3OH_2^+$ (*m/z* 33, [8]) at nearly the same photon energy. This is consistent with the findings of Shao et al. and Xie et al.[31-32] The asymmetric fragment ion TOF peaks of both of these ions are indicative of slow dissociation and their double-exponential shape implies isomerization of the molecular ion, as also noted by Shao et al.[31] To make sure that this is indeed the case, we first assumed direct dissociation for both fragment ions in the statistical model, which resulted in an unacceptable fit even when the transition states were set unreasonably tight. Therefore, isomerization was also included in the final model, similar to the 1-butanol model. In this case, as discussed in detail in the computational section, a hydrogen atom shifts from the methine group to the hydroxyl through a barrier at 10.50 eV and the resulting water is coordinated in a bridging position. Water is lost from this complex to form isobutene [6] fragment ion. From the best fit to the experimental data, a 0 K appearance energy of 10.57 ± 0.05 eV was obtained, which is in reasonable agreement with our G4 calculated value for the hydrogen transfer transition state. These results are in contrast to Shao et al.,[31] who suggested that methylcyclopropane ion is the only contributor to the *m/z* 56 channel. However, methylcyclopropane ion [4] could be formed if the hydrogen is transferred from one of the methyl groups, then the two CH_2 moiety close the three-membered ring. According to our calculations, the distance of these aforementioned CH_2 groups from each other is approximately 2.5 Å. The ring closure proceed through a barrier at 10.64 eV. This TS is nearly 1 eV higher than the experimental E_0, therefore this ion most likely does not contribute to the *m/z* 56 signal at threshold (Figure 8). The $CH_3OH_2^+$ [8] fragment ion comes from a different ion-neutral complex, where one of the methyl hydrogens is transferred to the hydroxyl group, then the other methyl group migrates to the water moiety to form the protonated methanol fragment ion. The 0 K appearance energy of $CH_3OH_2^+$ was determined to be 10.61 ± 0.02 eV, which is in good agreement with the G4 thermochemical limit of 10.62 eV, indicating a submerged barrier corresponding to the methyl migration.

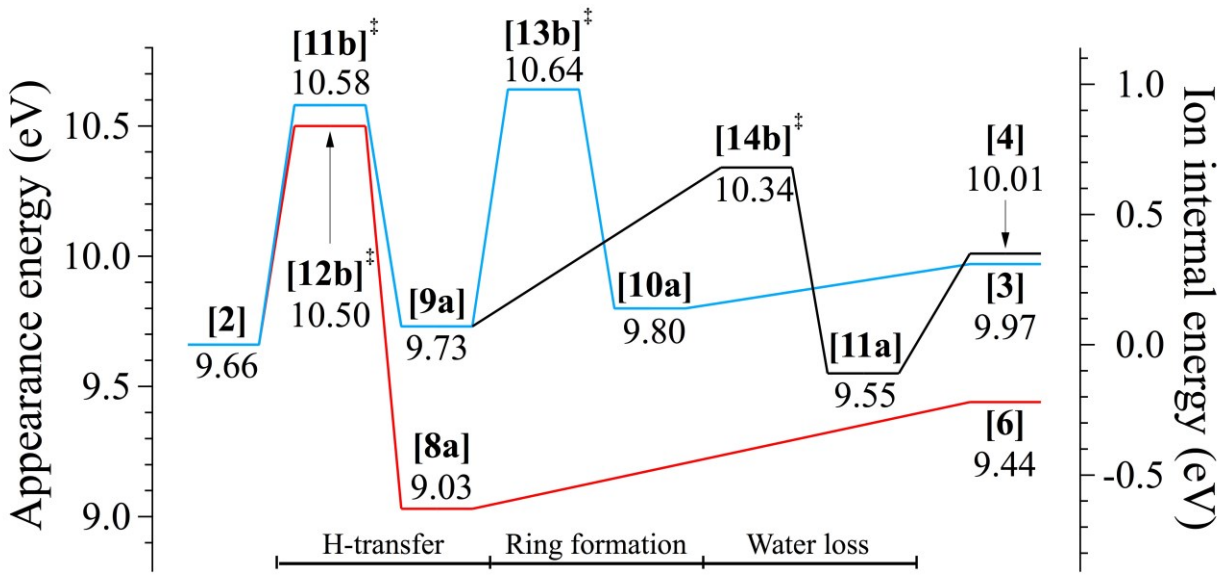

Figure 8. Potential energy surface for the internal hydrogen rearrangement and subsequent water loss from energy-selected isobutanol ions. Beta and gamma hydrogen transfers are shown with red and blue ink, respectively, and black lines show the methylcyclopropane formation through ring closure. Energies on the left axis are relative to the neutral precursor while energies on the right axis are relative to the molecular ion. For structures, see Figures 10, 12, and the schemes in the text.

The next fragment ion, $C_3H_6^+$ (*m/z* 42, [7]) is formed by methanol loss from the molecular ion and quickly overtakes both previous channels and accounts for the highest ion abundance between 11.4 and 11.9 eV. To rationalize the methanol loss, the simplest explanation is that the hydroxyl group shifts to one of the methyl groups, which induces the barrierless loss of CH_3OH neutral fragment, forming a propene, $CH_3CHCH_2^+$ cation in the process. Most likely, the flat, roaming OH transition state region lies below the dissociation threshold as the experimental E_0 of 10.72 ± 0.02 eV is in good agreement with the calculated thermochemical limit of 10.77 eV.

The abundance of the $C_3H_7^+$ (*m/z* 43, [9]) ion, formed by direct CH_2OH loss, steadily rises after ~11 eV and becomes the dominant channel above 12 eV. Contrary to 1-butanol, where an internal hydrogen shift was required to form the more stable CH_3CHCH_3 structure, it is directly available from the isobutanol molecular ion by a simple bond rupture. The experimental 0 K appearance energy was found to be 10.97 ± 0.05 eV, slightly lower than the G4-calculated thermochemical limit of 11.09 eV and in reasonable agreement with the ATcT value of 11.035 ± 0.010 eV. Similar to the case of 1-butanol, the corresponding heterolytic bond breakage is also possible, and the CH_2OH^+ (*m/z* 31, [10]) fragment ion appears as a minor dissociation channel at 11.2 eV, with a maximum of 15% abundance by 13.2 eV. The branching ratios between these two complementary channels are in contrast to our observations for 1-butanol, where the abundances of these channels are comparable: $C_3H_7^+$ [9] is 40%, and CH_2OH^+ [10] reaches its maximum just below 30%. This is another argument for a qualitatively different dissociation mechanism between the two systems and the common transition state that both dissociations go

through is responsible for the similar branching ratios between the homolytic and heterolytic cleavage in the 1-butanol ion. In isobutanol, the experimental E_0 of CH_2OH^+ was determined to be 11.11 ± 0.20 eV, in agreement with the ATcT and G4 calculated values of 11.145 ± 0.011 eV and 11.15 eV, respectively.

The final dissociation channel from isobutanol ions in the studied photon energy range is the consecutive formation of the $C_3H_5^+$ (*m/z* 41, [11]) cation by a methyl loss from *m/z* 56, with a maximum intensity of 5%. The abundance of this channel is so small that it could not be modeled reliably and it was excluded from the model. The visual appearance energy of $C_3H_5^+$ is between 11.6 and 11.9 eV, in agreement with the calculated G4 E_0 of 11.73 eV.

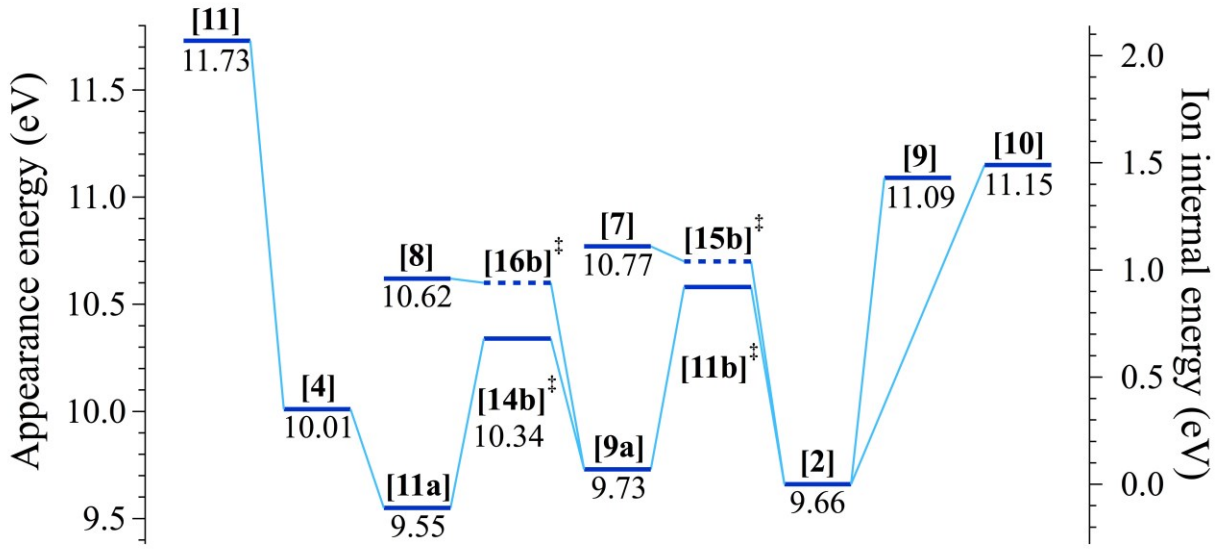

Figure 9. G4-calculated potential energy surface for the remaining dissociation pathways of energy-selected isobutanol ions. Energies on the left axis are relative to the neutral precursor while energies on the right axis are relative to the molecular ion. For structures, see Figures 10, 11, 12, and the schemes in the text.

Calculated dissociation mechanisms

Quantum chemical calculations were carried out to assist in the identification of the unimolecular dissociation pathways and quantify their energetics. Stationary points that are likely to play a role in the ionic dissociation processes were optimized at the B3LYP/6-311G++(d,p) level of theory. The stationary point energies were refined using the G4[57] composite method (Figures 4, 5, 8, and 9). All G4 energies are reported relative to the corresponding neutral butanol isomers.

1-Butanol. The first dissociation channel of the 1-butanol molecular ion [1] leads to the formation of $C_4H_8^+$ [3–6] by a water loss that, as we discussed in the previous section, requires the rearrangement of the molecular ion. We explored hydrogen atom transfers to the OH group

from the α-, β-, γ-, and δ-carbon atoms. The α-carbon hydrogen shift proceeds through a transition state at 11.28 eV, well above the experimental E_0 of 10.347 ± 0.015 eV. The hydrogen on the β-carbon can also be transferred in a single step through a transition state at 10.70 eV, leading to an ion-molecule complex between water and a 1-butene ion with an O···C distance of 2.279 Å. This complex is 0.39 eV more stable than the 1-butanol molecular ion itself and water is lost along a purely attractive potential energy curve, forming 1-butene.

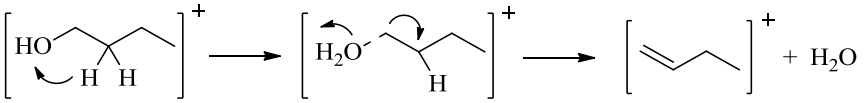

[**1**] [**3a**] [**4**]

Scheme 2. Formation of 1-butene ion (*m/z* 56) via a β-hydrogen transfer, followed by water loss.

In H-atom shift from the γ-carbon, the CH_2OH moiety rotates closer to the H donor site and the hydrogen transfer proceeds through a barrier of 10.42 eV, while the carbon chain assumes a cyclic structure. Then, through a second saddle point at 9.87 eV, water is lost, resulting in methylcyclopropane ion at a G4 thermochemical limit of 9.87 eV. Similarly to the β-carbon transfer, the ion–neutral complex, with an O···C distance of 2.431 Å, is 0.35 eV more stable than the parent ion.

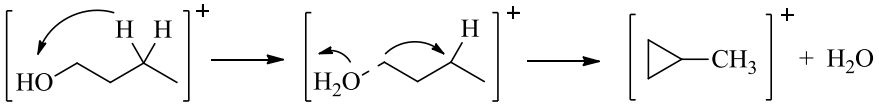

[**1**] [**5a**] [**3**]

Scheme 3. Formation of methylcyclopropane ion (*m/z* 56) via a γ-hydrogen transfer followed by water loss.

As a fourth possible pathway, the δ-carbon hydrogen shift corresponds to a McLafferty rearrangement.[67] To form the six-membered ring structure, the CH_2OH moiety of 1-butanol ion is rotated to an H–O–C_α–C_β dihedral angle of 92° through a barrier of 10.00 eV and the actual hydrogen transfer occurs via a transition state at 9.90 eV. The α- and γ-carbon atoms get closer to form the cyclobutane ring through a TS at 10.82 eV. While the barrier to the cyclobutane-water complex is lower than the transition states mentioned above, this ion-molecule complex is actually higher in energy than the 1-butanol cation by 0.18 eV.

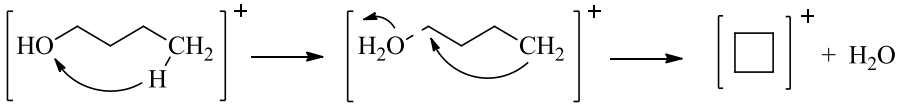

[**1**] [**4a**] [**5**]

Scheme 4. Formation of cyclobutane ion (*m/z* 56) via a δ-hydrogen transfer followed by water loss.

From here, water is lost directly at the thermochemical limit of 10.44 eV, which is higher in energy than the methylcyclopropane fragment ion channel. Because of this, the *m/z* 56 ion is most likely methylcyclopropane [3] at low energies but, at higher energies, dissociation to

cyclobutane ion [5] is also possible. Therefore, as discussed in length in the previous section, the source of the *m/z* 41 ion [11] is most likely 1-butene ion [4] formed through the β-carbon H-shift. The structure of the $C_3H_5^+$ ion is $CH_2CHCH_2^+$ formed by a methyl loss without a saddle point from 1-butene ion at 11.63 eV.

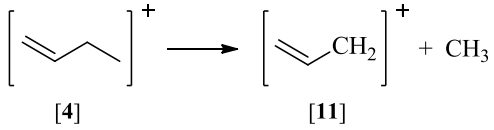

[4] [11]

Scheme 5. Formation of allylium ion (*m/z* 41) from 1-butene ion (*m/z* 56) via a methyl radical loss.

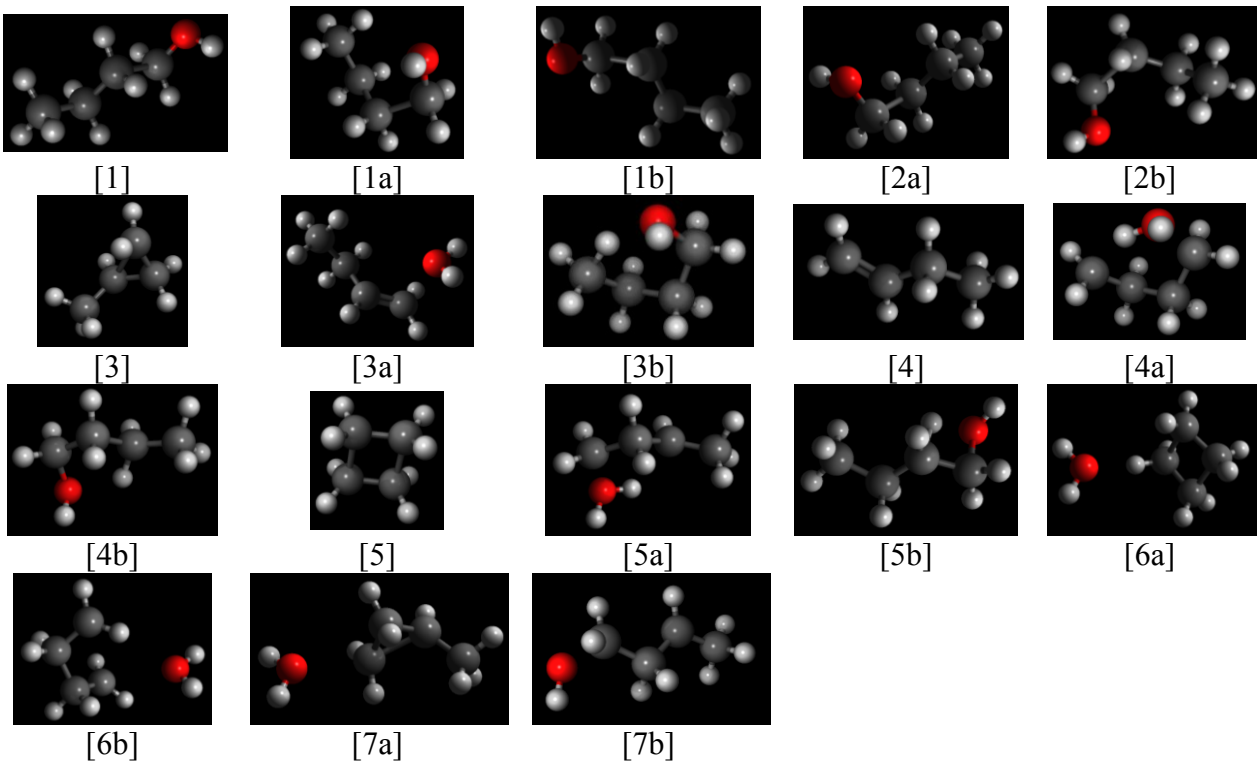

Figure 10. Structures of minima and saddle points as indicated in Figure 4.

Although our quantum chemical calculations did not account for direct hydrogen exchange, the water moiety may roam around in the ion-neutral complex, facilitating hydrogen exchange, supporting the conclusions of an early deuteration study by McAdoo and Hudson.[30]

The next ion in the breakdown diagram, $C_3H_6^+$ [7], is the product of a methanol loss. The lowest energy pathway is the γ-carbon hydrogen transfer to the α-carbon followed by the barrierless loss of the CH_3OH fragment. Hydrogen migration proceeds through a barrier at 10.87 eV and the system falls into a minimum structure where the α- and β-carbon atoms are separated by a bridging hydrogen atom. At this point, methanol is in a loose ion–neutral complex with the

$CH_3CHCH_2^+$ molecular ion. The α-carbon–hydrogen and β-carbon–hydrogen distances are 1.283 Å and 1.445 Å, respectively, and a C_α–H–C_β angle of 169º.

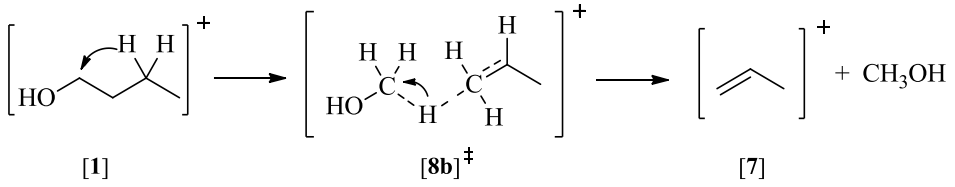

[**1**] [**8b**]‡ [**7**]

Scheme 6. Formation of propene ion (*m/z* 42) via a methanol loss.

It is evident that the *m/z* 33 ion, $CH_3OH_2^+$ [8], cannot be formed without substantial rearrangement of the molecular ion. The first step is the β-carbon hydrogen transfer to the OH group at 10.70 eV, which is the same initial step that we saw in the higher-energy water-loss channel. Then, the methyl group and water molecule form protonated methanol over a transition state and the CH_2CHCH_2 fragment is lost. Optimizations of this TS structure have not converged.

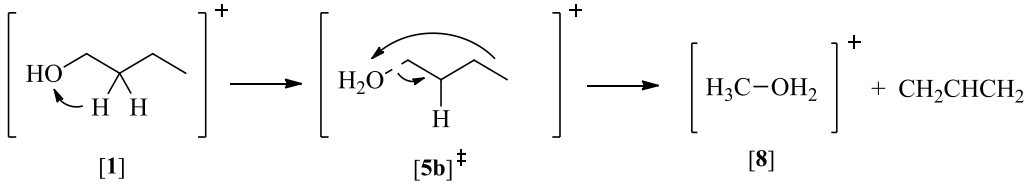

[**1**] [**5b**]‡ [**8**]

Scheme 7. Formation of methyloxonium ion (*m/z* 33) via an allyl radical loss.

The last two ions observed in our experiments, CH_2OH^+ [10] and $C_3H_7^+$ [9], could theoretically be formed by a simple bond rupture of 1-butanol. To confirm or reject this, constrained potential energy scans along the C_α–C_β bond length were performed on the molecular ion and no saddle point was located at the B3LYP level of theory. This means that CH_2OH^+ + $CH_3CH_2CH_2$ and $CH_3CH_2CH_2^+$ + CH_2OH can be formed at the respective thermochemical limits of 11.17 eV and 11.34 eV. However, both values are higher than the experimental appearance energies of 11.10 ± 0.03 eV. However, if a γ-hydrogen is transferred to the β-carbon, the energetically more stable CH_3CHCH_3 moiety may be formed. At the G4 level, the saddle point corresponding to hydrogen transfer is at 11.00 eV; slightly higher than the thermochemical threshold for $CH_3CHCH_3^+$ (10.99 eV) and slightly lower than the calculated threshold for CH_2OH^+ (11.05 eV).

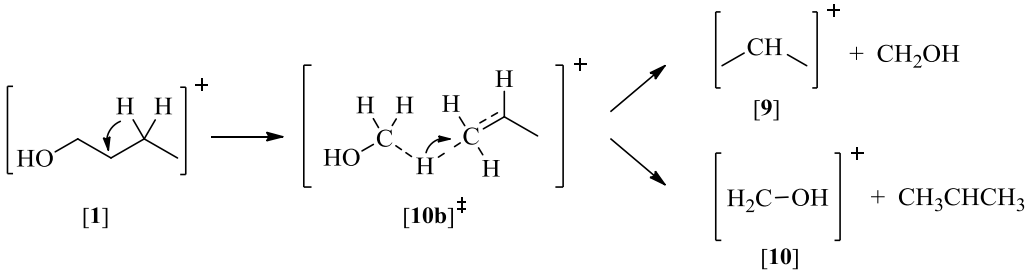

[**1**] [**10b**]‡ [**9**] [**10**]

Scheme 8. Formation of isopropylium (*m/z* 43) and hydroxymethylium (*m/z* 31) ions.

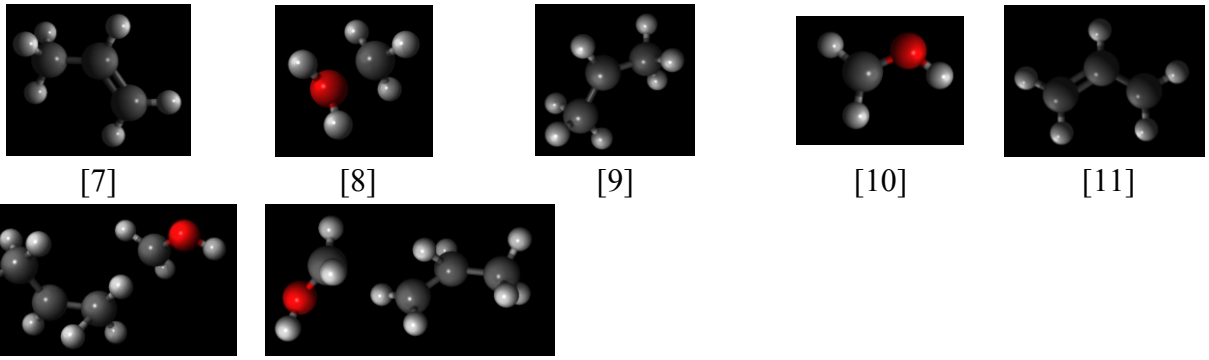

Figure 11. Structures of minima and saddle points as indicated in Figure 5.

Isobutanol. The first dissociation channel is the formation of $C_4H_8^+$ by water loss, which also requires the rearrangement of the molecular ion. We explored hydrogen atom transfers to the OH group both from the CH and CH_3 groups. The methine hydrogen is transferred in a single step through a barrier at 10.50 eV, forming isobutene, $CH_2=C(CH_3)CH_3^+$ molecular ion after the successive water loss without a saddle point.

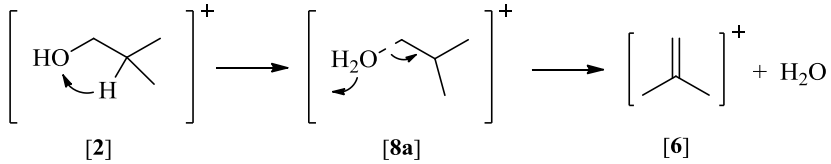

Scheme 9. Formation of isobutene (*m/z* 56) via water loss.

In the case of the methyl hydrogen shift, the transfer happens through a saddle point at 10.58 eV. This ion–molecule complex has a 4-membered ring, which is significantly more strained than the ones formed in the case of 1-butanol, with a O···C bond distance of only 1.547 Å. At this point, there are two possibilities: (1) losing the water or (2) forming a three-membered ring. In the first case, water is lost through a barrier at 10.34 eV, while the molecular ion undergoes a rearrangement via a methyl migration, forming 1-butene molecular ion.

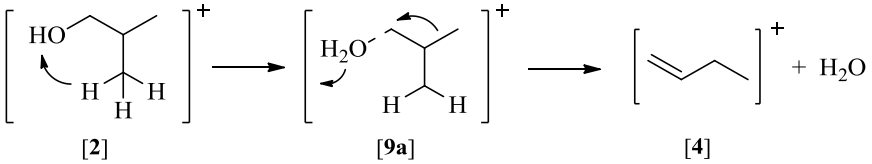

Scheme 10. Formation of 1-butene (*m/z* 56) after internal rearrangement.

In the other pathway, the α- and γ-carbon atoms move closer to each other, forming a cyclopropane ring through a barrier of 10.64 eV. Then, water is lost without a saddle point,

forming methylcyclopropane molecular ion with a similar thermochemical limit as in the case of [4].

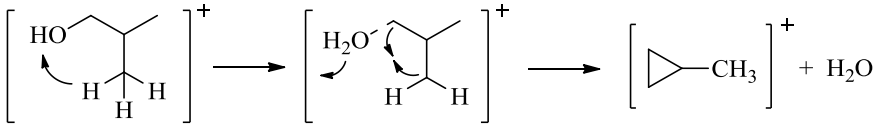

[2] [10a] [3]

Scheme 11. Formation of methylcyclopropane (*m/z* 56) via ring closure.

Since the ring closure step proceeds through a higher-lying transition state than for 1-butene (see Scheme 10), the most likely second contributor to the *m/z* 56 signal is 1-butene ion but this latter channel leading to methylcyclopropane ion cannot be ruled out, either.

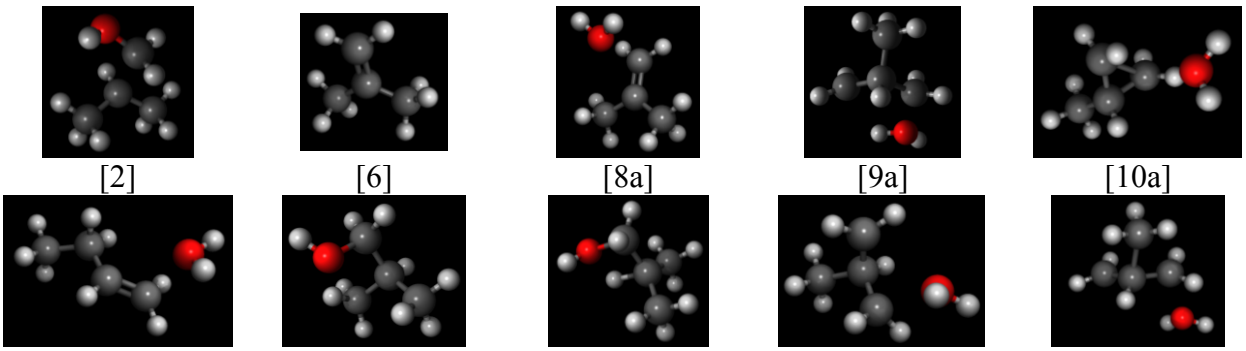

Figure 12. Structures of minima and saddle points as indicated in Figure 9.

The next fragment ion, namely $CH_3OH_2^+$, is formed by C_3H_5 loss. Its formation requires substantial rearrangement within the molecular ion. First, a hydrogen atom is transferred from one of the methyl groups to the hydroxyl group at 10.58 eV, similarly to the water loss channel. Then, the other methyl group and the water moiety form the protonated methanol ion. The remaining neutral, which has a CH_2CHCH_2 structure, leaves without a reverse barrier.

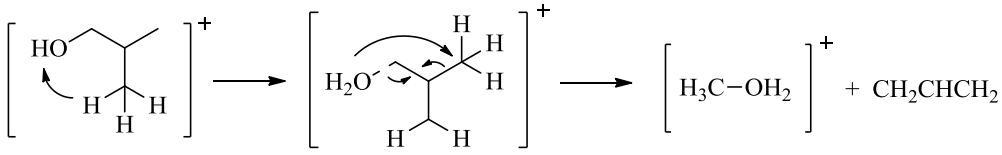

[2] [16b]‡ [8]

Scheme 12. Formation of the methyloxonium ion (*m/z* 33).

The next ion in the breakdown diagram, $C_3H_6^+$, is formed via a methanol loss and the dissociation mechanism is similar to the $CH_3OH_2^+$ channel. In this case, one of the methyl groups moves closer to the hydroxyl group, forming a CH_3OH group, which leaves without a

reverse barrier, forming the $CH_3CHCH_2^+$ fragment ion at a thermochemical threshold of 10.77 eV. Another possibility involving the transfer of a methyl hydrogen to the α-carbon was ruled out as it only resulted in an internal rearrangement of the molecular ion. The hydroxyl group moves to the place of the transferred hydrogen atom, yielding isobutanol in the end.

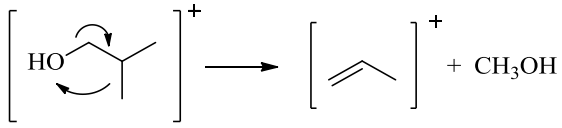

[**2**] [**7**]

Scheme 13. Formation of propene ion (*m/z* 42) via methanol loss.

$C_3H_7^+$ is the dominant channel in the breakdown diagram above 12.0 eV. Contrary to 1-butanol, there is no need for rearrangement to form the energetically favorable CH_3CHCH_3 structure. Constrained potential energy scans along the C_α–C_β bond length in the isobutanol molecular ion showed no saddle point, forming the energetically favored $C_3H_7^+$ ion at 11.09 eV, or forming CH_2OH^+ at 11.15 eV, which latter is only a minor product, contrary to the analogous dissociation from the 1-butanol ion.

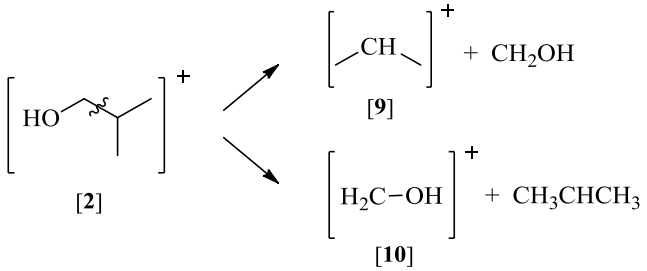

[**2**] [**9**] [**10**]

Scheme 14. Formation of isopropylium ion (*m/z* 43) and hydroxymethylium ion (*m/z* 31) via a bond rupture.

Finally, $C_3H_5^+$ is formed by a sequential CH_3 loss from 1-butene molecular ion without a saddle point at 11.73 eV.

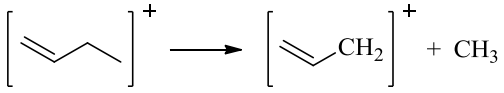

[**4**] [**11**]

Scheme 15. Formation of the allylium ion (*m/z* 41) from the 1-butene ion (*m/z* 56) via a methyl radical loss.

Thermochemistry

In the absence of a reverse barrier (that is, along an attractive reaction energy curve over a loose transition state), appearance energies represent the thermochemical limits leading to the ionic and neutral products. Therefore, the 0 K heat of formation of the 1-butanol and isobutanol can be calculated by using well-known literature thermochemical data on the fragment ions and

neutrals and the appearance energies extracted from the modeled breakdown diagrams. Ancillary thermochemical data and the results of this work are summarized in Table 2.

Table 2. Auxiliary and derived thermochemical data.

Chemical formula	Species	$\Delta_f H^{\circ}_{0\ K}$	$\Delta_f H^{\circ}_{298\ K}$	
		kJ mol^{-1}		
$C_4H_{10}O$	1-butanol	–245.81[c]		
			–274.4[d]	
			–274.9[e]	± 0.4
	isobutanol	–249.4[a]	–279.1[a]	± 1.6
			–283.8[d,f]	± 0.8
			–284.1[e]	± 0.9
$C_3H_7^+$	$CH_3CH^+CH_3$	822.91[b]		± 0.25
	$CH_3CH_2CH_2^+$	856.96[b]		± 0.86
C_3H_7	CH_3CHCH_3	105.32[b]		± 0.53
	$CH_3CH_2CH_2$	118.34[b]		± 0.55
CH_3O^+	CH_2OH^+	717.9[b]		± 0.7
		717.70[b]		± 0.18
CH_3O	CH_2OH	–11.1[b]		± 0.9
		–10.46[b]		± 0.28

[a] This work; [b] ATcT[68]; [c] Yaws[26]; [d] Rosenstock et al.[25]; [e] Pedley et al.[24]; [f] Connett.[27]

In the studied energy range, every dissociative photoionization pathway of 1-butanol and most isomerization pathways of isobutanol proceed through various higher-lying transition states, which means that the appearance energies do not correspond to the thermochemical limits. This prevents us from using these experimental appearance energies to extract reliable and accurate thermochemical information. However, there is one, rather prominent channel in isobutanol dissociative photoionization where the rearrangement transition state is submerged and the appearance energy does correspond to the thermochemical limit, and this is the $CH_3CHCH_2^+$ + CH_3OH channel. Combining this with the E_0s of $C_3H_7^+$ and CH_2OH^+ channels, we can calculate the isobutanol 0 K heat of formation reliably from three different channels. The extracted appearance energy for $CH_3CHCH_2^+$ + CH_3OH dissociation is 10.72 ± 0.02 eV. The ATcT[68] reports $\Delta_f H^{\circ}_{0\ K}$ of 975.22 ± 0.21 kJ mol^{-1} for the propylene ion and –190.01 ± 0.15 kJ mol^{-1} for methanol, which gives –249.40 ± 1.76 kJ mol^{-1} for the 0 K enthalpy of formation of isobutanol. The second channel is for $CH_3CHCH_3^+$ + $CH_2OH^{\bullet}$ dissociation with a E_0 of 10.97 ± 0.05 eV. Using the heats of formations found in ATcT[68] as 822.91 ± 0.25 kJ mol^{-1} for the ion and –10.46 ± 0.28 kJ mol^{-1} for the radical, we obtain a 0 K heat of formation of isobutanol as –245.99 ± 4.84 kJ mol^{-1}. Finally, the complimentary pair of the former dissociation, CH_2OH^+ + CH_3CHCH_3, is used in a similar fashion with ATcT heats of formations of 717.70 ± 0.18 kJ mol^{-1} for the ion and 105.32 ± 0.53 kJ mol^{-1} for the radical. The isobutanol heat of formation is calculated to be –248.0 ± 19.3 kJ mol^{-1}. The weighted average, as described by Shuman et al.,[69] of all three values

is calculated to be –249.00 ± 1.64 kJ mol^{-1}. To compare the evaluated enthalpy of formation of isobutanol with literature values, we converted our 0 K value to 298 K. The conversion factor ($H_{298\,K} - H_{0\,K}$) was carefully calculated to be 20.7 kJ mol^{-1} by Bodi et al.,[70] who took internal methyl rotation of isobutanol into account. Therefore, we obtain –279.10 ± 1.64 kJ mol^{-1} as the 298 K heat of formation of isobutanol. Connett[27] and Rosenstock[25] reported –283.8 kJ mol^{-1} and –283.8 ± 0.9 kJ mol^{-1}, respectively, as the gas phase heat of formation of isobutanol at 298 K, while Pedley et al.[24] gave –284.1 ± 0.9 kJ mol^{-1} at the same temperature. These old literature enthalpy of formation values do not match our result, and we propose a significant correction.

Conclusions

The unimolecular dissociation mechanism of internal energy selected 1-butanol and isobutanol cations was investigated by imaging photoelectron photoion coincidence spectroscopy using VUV synchrotron radiation. Both butanol isomer cations dissociate by numerous parallel and consecutive dissociation channels producing fragment ions with the same mass-to-charge ratios at *m/z* 31, 33, 41, 42, 43, and 56. Of these, we detected the fragment ions *m/z* 33 and 43 in 1-butanol, as well as *m/z* 31 and 41 in isobutanol for the first time. Despite the same set of fragment masses, the fractional ion abundances showed a fundamentally different behavior for the two isomers when plotted in the breakdown diagrams. We compare the dissociation mechanisms of the two isomers channel by channel as unveiled by statistical modeling of the experiment, aided by high-level quantum chemical calculations.

Both 1-butanol and isobutanol parent ions are metastable at low energies and the first dissociative ionization channel is water loss in at the 0 K appearance energy of 10.347 ± 0.015 eV and 10.57 ± 0.05 eV from 1-butanol and isobutanol, respectively. Both channels involve an initial isomerization step forming loose $C_4H_8^{+\cdots}H_2O$ ion–neutral complexes. However, in 1-butanol, this is formed by a γ-carbon H-atom shift, which produces the methylcyclopropane fragment ion (*m/z* 56, [3]) upon dissociation. In isobutanol, the intermediate complex is formed by a β-carbon H-atom shift and subsequent water loss yields the isobutene fragment ion (*m/z* 56, [6]). The most striking difference between the two isomers is that the H_2O-loss channel dominates the 1-butanol breakdown diagram in a wide photon energy range while it only appears as a minor pathway for isobutanol. We can explain this by considering the tightness (i.e., the activation entropy) of the H-shift transition state. In 1-butanol, this rearrangement involves a 5-membered ring structure ($\Delta S^{\ddagger}_{600K}$ = 18.2 J K^{-1} mol^{-1}), whereas in isobutanol, it requires a much more constrained 4-membered ring structure ($\Delta S^{\ddagger}_{600K}$ = –43.1 J K^{-1} mol^{-1}). Therefore, in isobutanol, the water-loss channel is quickly overtaken by the kinetically more favorable $CH_3OH_2^+$ channel.

For 1-butanol, the $CH_3OH_2^+$ (*m/z* 33, [8]) channel only reaches ~10% maximum abundance. The formation of this cation proceeds through a transition state at 10.74 ± 0.09 eV, which is higher than that of the water-loss channel and it is also less favored kinetically, with a fitted activation entropy of 2.0 J K^{-1} mol^{-1}. An initial hydrogen shift from the β-carbon to the

OH group forms a $C_4H_8^{+\cdots}H_2O$ complex, then the methyl group grabs this loosely bound water and leaves. For isobutanol, however, the breakdown diagram is dominated by this cation in the 10.4–11.3 eV photon energy range, due to its higher activation entropy (17.1 J K^{-1} mol^{-1}) and looser transition state compared with the water loss transition state. This channel is also slow at the dissociation limit and involves a H-atom shift from a methyl to the hydroxyl group, forming an ion–neutral complex, which dissociates to $CH_3OH_2^+$ and C_3H_5 through a submerged reverse barrier. The 0 K appearance energy of $CH_3OH_2^+$ from isobutanol was determined to be 10.61 ± 0.02 eV, in excellent agreement with the G4 calculated thermochemical limit of 10.62 eV.

The next channel in the 1-butanol breakdown diagram, amounting to 25% at its maximum, is the formation of $C_3H_6^+$ (*m/z* 42, [7]) by CH_3OH loss. The lowest energy $CH_3CH{=}CH_2^+$ structure can be formed by an internal H-shift from the γ- to the β-carbon over a reverse barrier, prior to the loss of CH_3OH without a reverse barrier. The 0 K appearance energy is 10.94 ± 0.04 eV. In isobutanol, CH_3OH loss is the dominant channel between 11.4–11.8 eV, with a maximum abundance of 45% and an appearance energy of 10.72 ± 0.02 eV. The stable propenyl cation, $CH_3CH{=}CH_2^+$, is easily accessible in isobutanol by C–O bond formation between the methyl and hydroxyl groups, while the analogous mechanism in 1-butanol would lead to the higher-energy cyclopropane (*c*-$CH_2CH_2CH_2^+$) cation and is energetically disallowed.

The $C_3H_7^+$ (*m/z* 43, [9]) and CH_2OH^+ (*m/z* 31, [10]) cations represent complementary pairs. The most stable $CH_3CHCH_3^+$ structure requires an H transfer in 1-butanol but is directly accessible in isobutanol. Indeed, in 1-butanol, despite an ionization energy difference between the two fragments of 0.11 eV,[68] the appearance energies of these two fragments are equal within the experimental uncertainty. Therefore, the dissociation is proposed to proceed through a common transition state at 11.10 ± 0.03 eV, slightly above the thermochemical limit, and the partitioning of the reactive flux, *i.e.,* the charge carrying fragment, is determined by the reaction dynamics past the transition state. In contrast, the $C_3H_7^+$ (*m/z* 43) and CH_2OH^+ (*m/z* 31) fragment ions are formed by direct C–C bond cleavage from isobutanol with appearance energies of 10.97 ± 0.05 and 11.11 ± 0.20 eV, respectively, reproducing the calculated ionization energy difference well. Thus, we can think of the production of one or the other charged fragment as two independent statistical fragmentation channels competing with each other. The proposed mechanisms are also confirmed by the fact that, in 1-butanol, the maximum abundances of the two fragment ions are similar at 40% for $C_3H_7^+$ [9] and 30% for CH_2OH^+ [10], while in isobutanol the $C_3H_7^+$ [9] channel dominates with a maximum abundance of ca. 70%, whereas CH_2OH^+ [10] is only a minor channel at 15%.

Finally, a consecutive dissociation channel opens up around 11.7–11.9 eV in both butanol isomers, consistent with the formation of $C_3H_5^+$ (*m/z* 41, [11]) by a consecutive loss of a methyl group from the H_2O-loss fragment ion. This consecutive channel amounts to about 15% in 1-butanol and only a few percent in isobutanol, consistent with the relative abundance of the parent water-loss channel between the two isotopes. Since water loss is possible through more than one mechanism, an accurate statistical modeling of this consecutive dissociation was not possible with any practical fidelity.

The surprisingly dissimilar and complex dissociation mechanism of the two butanol isomers 1-butanol and isobutanol could thus be revealed using photoelectron photoion coincidence spectroscopy supported by statistical modeling and quantum chemical calculations. The dissociation channels leading to the same *m*/*z* fragment ions were generally found to be distinct and their differing tightness and threshold energy explains the differences in the breakdown diagram. The isomer-dependent dissociative photoionization channels imply that the phase space of the two isomer ions is well-separated and the shared ion mass channels are mostly due to the limited number of energetically favorable fragmentation products of $C_4H_{10}O^+$.

Acknowledgements
This work has been funded by the National Science Foundation (Grant No. CHE-1665464) and by the Swiss Federal Office for Energy (BFE Contract No. SI/501269-01). Experiments were performed at the VUV beamline at the Swiss Light Source, Paul Scherrer Institute.

References

1. Kohse-Höinghaus, K.; Oßwald, P.; Cool, T. A.; Kasper, T.; Hansen, N.; Qi, F.; Westbrook, C. K.; Westmoreland, P. R., Biofuel Combustion Chemistry: From Ethanol to Biodiesel. *Angew. Chem., Int. Ed.* **2010**, *49*, 3572–3597.
2. Nigam, P. S.; Singh, A., Production of Liquid Biofuels from Renewable Resources. *Prog. Energy Combust. Sci.* **2011**, *37*, 52–68.
3. Harper, M. R.; Van Geem, K. M.; Pyl, S. P.; Marin, G. B.; Green, W. H., Comprehensive Reaction Mechanism for *n*-Butanol Pyrolysis and Combustion. *Combust. Flame* **2011**, *158*, 16–41.
4. Cai, J.; Zhang, L.; Zhang, F.; Wang, Z.; Cheng, Z.; Yuan, W.; Qi, F., Experimental and Kinetic Modeling Study of *n*-Butanol Pyrolysis and Combustion. *Energy Fuels* **2012**, *26*, 5550–5568.
5. Gu, X.; Huang, Z.; Wu, S.; Li, Q., Laminar Burning Velocities and Flame Instabilities of Butanol Isomers–Air Mixtures. *Combust. Flame* **2010**, *157*, 2318–2325.
6. Veloo, P. S.; Egolfopoulos, F. N., Flame Propagation of Butanol Isomers/Air Mixtures. *Proc. Combust. Inst.* **2011**, *33*, 987–993.
7. Black, G.; Curran, H. J.; Pichon, S.; Simmie, J. M.; Zhukov, V., Bio-Butanol: Combustion Properties and Detailed Chemical Kinetic Model. *Combust. Flame* **2010**, *157*, 363–373.
8. Heufer, K. A.; Fernandes, R. X.; Olivier, H.; Beeckmann, J.; Röhl, O.; Peters, N., Shock Tube Investigations of Ignition Delays of *n*-Butanol at Elevated Pressures Between 770 and 1250K. *Proc. Combust. Inst.* **2011**, *33*, 359–366.
9. Stranic, I.; Chase, D. P.; Harmon, J. T.; Yang, S.; Davidson, D. F.; Hanson, R. K., Shock Tube Measurements of Ignition Delay Times for the Butanol Isomers. *Combust. Flame* **2012**, *159*, 516–527.
10. Moss, J. T.; Berkowitz, A. M.; Oehlschlaeger, M. A.; Biet, J.; Warth, V.; Glaude, P.-A.; Battin-Leclerc, F., An Experimental and Kinetic Modeling Study of the Oxidation of the Four Isomers of Butanol. *J. Phys. Chem. A* **2008**, *112*, 10843–10855.
11. Dagaut, P.; Sarathy, S. M.; Thomson, M. J., A Chemical Kinetic Study of *n*-Butanol Oxidation at Elevated Pressure in a Jet Stirred Reactor. *Proc. Combust. Inst.* **2009**, *32*, 229–237.
12. Sarathy, S. M.; Thomson, M. J.; Togbé, C.; Dagaut, P.; Halter, F.; Mounaim-Rousselle, C., An Experimental and Kinetic Modeling Study of *n*-Butanol Combustion. *Combust. Flame* **2009**, *156*, 852–864.
13. Yang, B.; Oßwald, P.; Li, Y.; Wang, J.; Wei, L.; Tian, Z.; Qi, F.; Kohse-Höinghaus, K., Identification of Combustion Intermediates in Isomeric Fuel-Rich Premixed Butanol–Oxygen Flames at Low Pressure. *Combust. Flame* **2007**, *148*, 198–209.
14. Hansen, N.; Harper, M. R.; Green, W. H., High-Temperature Oxidation Chemistry of *n*-Butanol – Experiments in Low-Pressure Premixed Flames and Detailed Kinetic Modeling. *Phys. Chem. Chem. Phys.* **2011**, *13*, 20262–20274.
15. Oßwald, P.; Güldenberg, H.; Kohse-Höinghaus, K.; Yang, B.; Yuan, T.; Qi, F., Combustion of Butanol Isomers – A Detailed Molecular Beam Mass Spectrometry Investigation of Their Flame Chemistry. *Combust. Flame* **2011**, *158*, 2–15.
16. Merchant, S. S.; Zanoelo, E. F.; Speth, R. L.; Harper, M. R.; Van Geem, K. M.; Green, W. H., Combustion and Pyrolysis of *iso*-Butanol: Experimental and Chemical Kinetic Modeling Study. *Combust. Flame* **2013**, *160*, 1907–1929.
17. Sarathy, S. M.; Vranckx, S.; Yasunaga, K.; Mehl, M.; Oßwald, P.; Metcalfe, W. K.; Westbrook, C. K.; Pitz, W. J.; Kohse-Höinghaus, K.; Fernandes, R. X.*, et al.*, A Comprehensive

Chemical Kinetic Combustion Model for the Four Butanol Isomers. *Combust. Flame* **2012**, *159*, 2028–2055.
18. Bose, D.; Wright, M.; Gökçen, T., Uncertainty and Sensitivity Analysis of Thermochemical Modeling for Titan Atmospheric Entry. *37th AIAA Thermophysics Conference* **2004**.
19. Raman, V.; Hassanaly, M., Emerging Trends in Numerical Simulations of Combustion Systems. *Proc. Combust. Inst.* **2019**, *37*, 2073–2089.
20. Zádor, J.; Zsély, I. G.; Turányi, T.; Ratto, M.; Tarantola, S.; Saltelli, A., Local and Global Uncertainty Analyses of a Methane Flame Model. *J. Phys. Chem. A* **2005**, *109*, 9795–9807.
21. Afeefy, H. Y.; Liebman, J. F.; Stein, S. E., Neutral Thermochemical Data. In *NIST Chemistry WebBook, NIST Standard Reference Database Number 69*, Linstrom, P. J.; Mallard, W. G., Eds., National Institute of Standards and Technology, Gaithersburg MD, 20899, (retrieved August 14, 2019).
22. Skinner, H. A.; Snelson, A., The Heats of Combustion of the Four Isomeric Butyl Alcohols. *Trans. Faraday Soc.* **1960**, *56*, 1776–1783.
23. Wadsö, I., Heats of Vaporization for a Number of Organic Compounds at 25 ºC. *Acta Chemica Scandinavica* **1966**, *20*, 544–552.
24. Pedley, J. B., *Thermochemical Data and Structures of Organic Compounds*. CRC Press: 1994; Vol. 1.
25. Rosenstock, H. M.; Draxl, K.; Steiner, B. W.; Herron, J. T., *Energetics of Gaseous Ions*. National Standard Reference Data System: 1977; p 783.
26. Yaws, C. L., *Yaws' Handbook of Thermodynamic and Physical Properties of Chemical Compounds*. Gulf Publishing Company: 2006; p 776.
27. Connett, J. E., Chemical Equilibria 6. Measurement of Equilibrium Constants for the Dehydrogenation of 2-Methylpropan-1-ol by a Vapour-Flow Technique. *J. Chem. Thermodynam.* **1975**, *7*, 1159–1162.
28. Voronova, K.; Ervin, K. M.; Torma, K. G.; Hemberger, P.; Bodi, A.; Gerber, T.; Osborn, D. L.; Sztáray, B., Radical Thermometers, Thermochemistry, and Photoelectron Spectra: A Photoelectron Photoion Coincidence Spectroscopy Study of the Methyl Peroxy Radical. *J. Phys. Chem. Lett.* **2018**, *9*, 534–539.
29. Covert, K. J.; Voronova, K.; Torma, K. G.; Bodi, A.; Zádor, J.; Sztáray, B., Thermochemistry of the Smallest QOOH Radical from the Roaming Fragmentation of Energy Selected Methyl Hydroperoxide Ions. *Phys. Chem. Chem. Phys.* **2018**, *20*, 21085–21094.
30. McAdoo, D. J.; Hudson, C. E., Ion- Neutral Complex- Mediated Hydrogen Exchange in Ionized *n*- Butanol: a Mechanism for 'Non- specific' Hydrogen Migrations. *Org. Mass Spectrom.* **1987**, *22*, 615–621.
31. Shao, J. D.; Baer, T.; Lewis, D. K., Dissociation Dynamics of Energy-Selected Ion-Dipole Complexes. 2. Butyl Alcohol Ions. *J. Phys. Chem* **1988**, *92*, 5123–5128.
32. Xie, M.; Zhou, Z.; Wang, Z.; Chen, D.; Qi, F., Determination of Absolute Photoionization Cross-Sections of Oxygenated Hydrocarbons. *Int. J. Mass Spectrom.* **2010**, *293*, 28–33.
33. Ahmed, M. S.; Hudson, C. E.; Giam, C. S.; McAdoo, D. J., Methylcyclopropane Ion Formation by Elimination of Water from *n*-Butanol and 2-Methylpropanol Ions. *Org. Mass Spectrom.* **1991**, *26*, 1089–1091.
34. Bowen, R. D.; Maccoll, A., Low Energy, Low Temperature Mass Spectra 2—Low Energy, Low Temperature Mass Spectra of Some Small Saturated Alcohols and Ethers. *Org. Mass Spectrom.* **1984**, *19*, 379–384.

35. Lambdin, W. J.; Tuffly, B. L.; Yarborough, V. A., Appearance Potentials as Obtained with an Analytical Mass Spectrometer. *Appl. Spectrosc.* **1959**, *13*, 71–74.
36. Selim, E. T. M.; Helal, A. I., Heat of Formation of CH_2=OH^+ Fragment Ion. *Indian J. Pure Appl. Phys.* **1981**, *19*, 977–982.
37. Bodi, A.; Stevens, W. R.; Baer, T., Understanding the Complex Dissociation Dynamics of Energy Selected Dichloroethylene Ions: Neutral Isomerization Energies and Heats of Formation by Imaging Photoelectron−Photoion Coincidence. *J. Phys. Chem. A* **2011**, *115*, 726–734.
38. Bodi, A.; Johnson, M.; Gerber, T.; Gengeliczki, Z.; Sztáray, B., Imaging Photoelectron Photoion Coincidence Spectroscopy with Velocity Focusing Electron Optics. *Rev. Sci. Instrum.* **2009**, *80*, 034101.
39. Johnson, M.; Bodi, A.; Schulz, L.; Gerber, T., Vacuum Ultraviolet Beamline at the Swiss Light Source for Chemical Dynamics Studies. *Nucl. Instrum. Methods Phys. Res. A* **2009**, *610*, 597–603.
40. Sztáray, B.; Baer, T., Suppression of Hot Electrons in Threshold Photoelectron Photoion Coincidence Spectroscopy Using Velocity Focusing Optics. *Rev. Sci. Instrum.* **2003**, *74*, 3763–3768.
41. Wiley, W. C.; McLaren, I. H., Time- of- Flight Mass Spectrometer with Improved Resolution. *Rev. Sci. Instrum.* **1955**, *26*, 1150–1157.
42. Bodi, A.; Sztáray, B.; Baer, T.; Johnson, M.; Gerber, T., Data Acquisition Schemes for Continuous Two-Particle Time-of-Flight Coincidence Experiments. *Rev. Sci. Instrum.* **2007**, *78*, 084102.
43. Sztáray, B.; Bodi, A.; Baer, T., Modeling Unimolecular Reactions in Photoelectron Photoion Coincidence Experiments. *J. Mass Spectrom.* **2010**, *45*, 1233–1245.
44. Baer, T.; Sztáray, B.; Kercher, J. P.; Lago, A. F.; Bodi, A.; Skull, C.; Palathinkal, D., Threshold Photoelectron Photoion Coincidence Studies of Parallel and Sequential Dissociation Reactions. *Phys. Chem. Chem. Phys.* **2005**, *7*, 1507–1513.
45. Benson, S. W., *Thermochemical Kinetics: Methods for the Estimation of Thermochemical Data and Rate Parameters*. 2nd Edition ed.; John Wiley & Sons, Inc.: New York, 1976.
46. Baer, T.; Hase, W. L., *Unimolecular Reaction Dynamics: Theory and Experiments*. Oxford University Press: New York, 1996.
47. Beyer, T.; Swinehart, D. F., AlgorithM 448: Number of Multiply-Restricted Partitions. *Commun. ACM* **1973**, *16*, 379.
48. Li, Y.; Baer, T., Ethylene Glycol Ions Dissociate by Tunneling through an H-Atom Transfer Barrier: A DFT and TPEPICO Study. *J. Phys. Chem. A* **2002**, *106*, 8658–8666.
49. Torma, K. G.; Voronova, K.; Sztáray, B.; Bodi, A., Dissociative Photoionization of the C_7H_8 Isomers Cycloheptatriene and Toluene: Looking at Two Sides of the Same Coin Simultaneously. *J. Phys. Chem. A* **2019**, *123*, 3454–3463.
50. Muller, G.; Voronova, K.; Sztáray, B.; Meloni, G., Rotamers and Migration: Investigating the Dissociative Photoionization of Ethylenediamine. *J. Phys. Chem. A* **2016**, *120*, 3906–3916.
51. Xiao, W.; Hu, Y.; Li, W.; Guan, J.; Liu, F.; Shan, X.; Sheng, L., Unexpected Methyl Migrations of Ethanol Dimer under Synchrotron VUV Radiation. *J. Chem. Phys.* **2015**, *142*, 024306.
52. Dyakov, Y. A.; Ni, C. K.; Lin, S. H.; Lee, Y. T.; Mebel, A. M., *Ab Initio* and RRKM Study of Photodissociation of Azulene Cation. *Phys. Chem. Chem. Phys.* **2006**, *8*, 1404–1415.

53. Jobst, K. J.; Jogee, S.; Bowen, R. D.; Terlouw, J. K., A Mechanistic Study of the Prominent Loss of H_2O from Ionized 2-Hydroxyaminoethanol. *Int. J. Mass Spectrom.* **2011**, *306*, 138–149.
54. Borkar, S.; Sztáray, B.; Bodi, A., Dissociating $C_3H_5Br^+$ Ions: Almost All Roads Lead to the Allyl Cation. *Int. J. Mass Spectrom.* **2012**, *330–332*, 100–108.
55. Daly, S.; Powis, I.; Tia, M.; Garcia, G. A.; Nahon, L., Dissociative VUV Photoionization of Butanediol Isomers. *Int. J. Mass Spectrom.* **2015**, *376*, 46–53.
56. Frisch, M. J.; Trucks, G. W.; Schlegel, H. B.; Scuseria, G. E.; Robb, M. A.; Cheeseman, J. R.; Scalmani, G.; Barone, V.; Mennucci, B.; Petersson, G. A.*, et al. Gaussian 09*, Gaussian, Inc.: Wallingford, CT, USA, 2009.
57. Curtiss, L. A.; Redfern, P. C.; Raghavachari, K., Gaussian-4 Theory. *J. Chem. Phys.* **2007**, *126*, 084108.
58. Peng, C.; Bernhard Schlegel, H., Combining Synchronous Transit and Quasi-Newton Methods to Find Transition States. *Isr. J. Chem.* **1993**, *33*, 449–454.
59. Peng, C.; Ayala, P. Y.; Schlegel, H. B.; Frisch, M. J., Using Redundant Internal Coordinates to Optimize Equilibrium Geometries and Transition States. *J. Comput. Chem.* **1996**, *17*, 49–56.
60. Montgomery, J. A. J.; Frisch, M. J.; Ochterski, J. W.; Petersson, G. A., A Complete Basis Set Model Chemistry. VI. Use of Density Functional Geometries and Frequencies. *J. Chem. Phys.* **1999**, *110*, 2822–2827.
61. Montgomery, J. A. J.; Frisch, M. J.; Ochterski, J. W.; Petersson, G. A., A Complete Basis Set Model Chemistry. VII. Use of the Minimum Population Localization Method. *J. Chem. Phys.* **2000**, *112*, 6532–6542.
62. Ochterski, J. W.; Petersson, G. A.; Montgomery Jr., J. A., A Complete Basis Set Model Chemistry. V. Extensions to Six or More Heavy Atoms. *J. Chem. Phys.* **1996**, *104*, 2598–2619.
63. Martin, J. M. L.; de Oliveira, G., Towards Standard Methods for Benchmark Quality Ab Initio Thermochemistry—W1 and W2 Theory. *J. Chem. Phys.* **1999**, *111*, 1843–1856.
64. Cocksey, B. J.; Eland, J. H. D.; Danby, C. J., The Effect of Alkyl Substitution on Ionisation Potential. *J. Chem. Soc. B: Phys. Org.* **1971**, 790–792.
65. Bodi, A.; Brannock, M. D.; Sztáray, B.; Baer, T., Tunneling in H Loss from Energy Selected Ethanol Ions. *Phys. Chem. Chem. Phys.* **2012**, *14*, 16047–16054.
66. Voronova, K.; Mozaffari Easter, C. M.; Covert, K. J.; Bodi, A.; Hemberger, P.; Sztáray, B., Dissociative Photoionization of Diethyl Ether. *J. Phys. Chem. A* **2015**, *119*, 10654–10663.
67. McLafferty, F. W., Mass Spectrometric Analysis Broad Applicability to Chemical Research. *Anal. Chem.* **1956**, *28*, 306–316.
68. Ruscic, B.; Bross, D. H. *Active Thermochemical Tables (ATcT)* values based on ver. 1.122e of the Thermochemical Network available at ATcT.anl.gov,
69. Shuman, N. S.; Zhao, L. Y.; Boles, M.; Baer, T.; Sztáray, B., Heats of Formation of $HCCl_3$, $HCCl_2Br$, $HCClBr_2$, $HCBr_3$, and Their Fragment Ions Studied by Threshold Photoelectron Photoion Coincidence. *J. Phys. Chem. A* **2008**, *112*, 10533–10538.
70. Bodi, A.; Kercher, J. P.; Bond, C.; Meteesatien, P.; Sztáray, B.; Baer, T., Photoion Photoelectron Coincidence Spectroscopy of Primary Amines RCH_2NH_2 (R = H, CH_3, C_2H_5, C_3H_7, *i*-C_3H_7): Alkylamine and Alkyl Radical Heats of Formation by Isodesmic Reaction Networks. *J. Phys. Chem. A* **2006**, *110*, 13425–13433.